Supporting Information for 'A Synthesis of Global Coastal Ocean Greenhouse Gas Fluxes'

L. Resplandy[1], A. Hogikyan[2], J. D. Müller[3], R. G. Najjar[4], H. W. Bange[5], D. Bianchi[6], T. Weber[7], Wei-Jun Cai[8], S.C. Doney[9], K. Fennel[10], M. Gehlen[11], J. Hauck[12], F. Lacroix[13], P. Landschützer[14], C. Le Quéré[15], A. Roobaert[14,16], J. Schwinger[17], S. Berthet[18], L. Bopp[19], T.T.T. Chau[9], M. Dai[20], N. Gruber[14], T. Ilyina[21], A. Kock[3]*, M. Manizza[22], Z. Lachkar[23], G. G. Laruelle[16], E. Liao[1]†, I.D. Lima[24], C. Nissen[12,25], C. Rödenbeck[26], R. Séférian[18], K. Toyama[27], H. Tsujino[27], P. Regnier[16]

[1]Department of Geosciences and High Meadows Environmental Institute, Princeton University, Princeton, NJ, USA
[2]Atmospheric and Oceanic Sciences Program, Princeton University, Princeton, NJ, USA
[3]Environmental Physics, Institute of Biogeochemistry and Pollutant Dynamics, ETH Zurich, Zürich, Switzerland
[4]Department of Meteorology and Atmospheric Science, The Pennsylvania State University, University Park, Pennsylvania, USA
[5]GEOMAR Helmholtz Centre for Ocean Research Kiel, Kiel, Germany
[6]Department of Atmospheric and Oceanic Sciences, University of California Los Angeles, Los Angeles, CA, USA
[7]Department of Earth and Environmental Science, University of Rochester, NY, USA
[8]School of Marine Science and Policy, University of Delaware, Newark, Delaware, 19716, USA
[9]Department of Environmental Sciences, University of Virginia, Charlottesville, VA, USA
[10]Department of Oceanography, Dalhousie University, Halifax, Canada
[11]Laboratoire des Sciences du Climat et de l'Environnement, LSCE/IPSL, CEA-CNRS-UVSQ, Université Paris-Saclay, F-91191 Gif-sur-Yvette, France
[12]Alfred-Wegener-Institut, Helmholtz-Zentrum für Polar- und Meeresforschung, Germany
[13]Climate and Environmental Physics / Oeschger Centre for Climate Change Research (OCCR), University of Bern, Switzerland
[14]Flanders Marine Institute (VLIZ), Ostend Belgium
[15]School of Environmental Sciences, University of East Anglia, Norwich Research Park, NR4 7TJ, Norwich, UK
[16]Dept. Geoscience, Environment and Society - BGEOSYS, Université Libre de Bruxelles, Brussels, Belgium
[17]NORCE Climate & Environment, Bjerknes Centre for Climate Research, Bergen, Norway
[18]CNRM, Université de Toulouse, Météo France, CNRS, Toulouse, France
[19]LMD/IPSL, ENS, Université PSL, École Polytechnique, Institut Polytechnique de Paris, Sorbonne Université, CNRS, Paris, France
[20]State Key Lab of Marine Environmental Science and College of Ocean and Earth Sciences, Xiamen University, Xiamen 361102, China
[21]Max Planck Institute for Meteorology, Hamburg, Germany
[22]Geosciences Research Division, Scripps Institution of Oceanography, University of California - San Diego, La Jolla, USA
[23]Arabian Center for Climate and Environmental Sciences, New York University Abu Dhabi, Abu Dhabi, United Arab Emirates
[24]Department of Marine Chemistry and Geochemistry, Woods Hole Oceanographic Institution, Woods Hole, MA, USA
[25]Department of Atmospheric and Oceanic Sciences and Institute of Arctic and Alpine Research, University of Colorado, Boulder, Colorado, USA
[26]MPI Biogeochemistry, Jena, Germany
[27]JMA Meteorological Research Institute, Tsukuba, Ibaraki, Japan

Contents of this file

*now at State Office for the Environment of the State of Schleswig-Holstein, Flintbek, Germany
†now at School of Oceanography, Shang Jiao Tong University, Shanghai, 200030, China

0886-6236/24/$12.00

Text S1. Observation-based products and models description

S1.a pCO_2-products

CMEMS-LSCE-FFNN (CMEMS)

The CMEMS-LSCE-FFNN product (Chau et al., 2022) referred to here as CMEMS provides estimates of monthly pCO_2 and air-sea CO_2 fluxes over the global coastal ocean at a spatial resolution of 1×1 degree from 1985 to 2018. Main characteristics setting CMEMS-LSCE-FFNN apart from similar approaches are (1) model design, (2) ensemble-based estimates of pCO_2 and air-sea CO_2 fluxes and uncertainty, and (3) consistency of the coastal-ocean reconstruction and the open-ocean reconstruction (Chau et al., 2022). Coastal estimates were evaluated thoroughly from a global scale to ocean basins and at time-series stations. The coastal estimates are part of a global reconstruction of pCO_2 fields based on monthly gridded SOCATv2020 data of CO_2 fugacity covering both the open ocean and the coastal zone (Bakker et al., 2016) (see Figure S1). The reconstruction is based on an ensemble of 100 feed-forward neural networks (FFNN), with two-thirds of SOCAT data used for model training and one third kept for validation of reconstructed pCO_2 . The ensemble approach provides space-time varying uncertainty field (ensemble spread) associated with the best pCO_2 and air-sea fluxes' estimates (ensemble mean). These ensemble statistics permit the evaluation of reconstruction uncertainty over coastal regions with sparse data coverage. The seamless reconstruction of pCO_2 and air-sea fluxes over the global coastal and open ocean allows the assessment of gradients and horizontal variability of pCO_2 and air-sea CO_2 fluxes over the continental shelf and to the open ocean. The gas transfer velocity was calculated with 10-m ERA5 wind speed data (Hersbach et al., 2020) following the parameterization by Wanninkhof (2014). A scaling factor is applied such that the global average of kw equals to 16.5 cm h^{-1} (Naegler, 2009). Air-sea CO_2 fluxes are also scaled proportional to CMEMS-OSTIA sea ice fraction over polar and subpolar regions (S. Good et al., 2020).

Coastal-SOM-FFN

The coastal air-sea CO_2 product (referred here as coastal-SOM-FFN) is based on the continuous coastal pCO_2 product of Laruelle et al. (2017) that used the Self-Organizing Map Feed Forward method developed by Landschützer et al. (2013) but adapted for the coastal ocean to fill region without data. The method in a first step clusters coastal ocean regions into dynamic biogeochemical provinces. In a second step, a non-linear regression step links physical, biological and chemical proxy data with existing CO_2 measurements. The coastal ocean is thereby explicitly reconstructed with coastal-only observations from the SOCATv4 database. The established regression relationship is then used to fill areas where no observations exist (a more detailed description can be found in Landschützer et al. (2013) and Laruelle et al. (2017). The coastal domain defined by Laruelle et al. (2017) excludes estuaries and inland water bodies with an outer limit defined as 300 km away from the shoreline (total surface area of 77 million km^2). This pCO_2-product is available as monthly 0.25-degree maps for the 1998-2015 period. The SST, SSS, wind product and sea-ice used to calculate the air-sea CO_2 exchange derived from the daily NOAA OI SST V2 (Reynolds et al., 2007), the daily Hadley center EN4 SSS (S. A. Good et al., 2013), the monthly second moment of the 6-hour 0.25° global atmospheric reanalysis ERA-interim wind product (Dee et al., 2011) and the monthly mean of the daily 0.25° sea-ice dataset of Reynolds et al. (2007), respectively. We use the equation developed by (Ho et al., 2011) to calculate the gas exchange transfer velocity.

Merged-SOM-FFN

The air-sea CO_2 flux product based on Landschützer et al. (2020) (referred here as Merged-SOM-FFN) is built on the combination of the open ocean CO_2 product by Landschützer et al. (2014) using SOCATv5 and the coastal ocean product by Laruelle et al. (2017) using SOCATv4 (referred here as Coastal-SOM-FFN), both created using the Self-Organizing Map Feed Forward Network (SOM-FFN) method developed by Landschützer et al. (2013). Open ocean regions in the original product are broadly defined as all waters 1 degree off shore, whereas the coastal ocean in Laruelle et al. (2017) includes all ocean areas within 300 km offshore following the SOCAT definition (Bakker et al., 2016), whereas the overlap area is merged by simple error statistics (Landschützer et al., 2020). The merged climatology, presented in Landschützer et al. (2020), is available globally on a 0.25x0.25 degree grid to better resolve fine coastal characteristics and covers coastal ocean regions, shelf seas, as well as marginal seas. The dataset used to calculate the air-sea CO_2 flux (i.e., SST, SSS, wind) is the same as described for the coastal-SOM-FFN product.

Carboscope-1

The Carboscope pCO_2 interpolation is normally run at a resolution of 2 x 2.5 degree (version oc_v2021, update of Rödenbeck et al. (2013)) but we use here a higher-resolution version of 1 x 1 degree (CarboScope RunID oc_1x1_v2021) to better resolve spatial details. As a secondary change for computational feasibility, the calculation period has been shortened, now starting in 1988, with the valid period starting in 1992. We note that the Bayesian a-priori uncertainty is set according to a global normalization condition, even though the pCO_2 constraint is a local one; thus the effective local regularization strength in the 1 x 1 version might be somewhat different compared to that in the regular 2.5 x 2 version. This version uses SOCAT version 2021, sea ice coverage is based on HadISST 2.2.0.0 (Titchner & Rayner, 2014). Wind speed are from JRA55-do v1.5.0 (Tsujino et al., 2018) used quadratically as in (Wanninkhof, 1992), and global mean piston velocity are scaled to 16.5 cm h^{-1} but the normalization of the gas transfer velocity to a global long-term average of 16.5 cm h^{-1} might lead to slight differences in the local transfer velocities.

S1.b N_2O and CH_4 observation-based products

MARCATS-N2O and MARCATS-CH4

MARCATS-N2O and MARCATS-CH4 are based on the collection of in-situ concentration data of N_2O and CH_4 from the MEMENTO (MarinE MethanE and NiTrous Oxide) data base (Kock & Bange, 2015) and were computed at the scale of the 45 MARgins and CATchments Segmentation (MARCATS) regions (Laruelle et al., 2013) (Figure S2). For each MARCATS region, N_2O and CH_4 surface (1 - 10 m) concentration data were extracted from MEMENTO. Individual DN2O and DCH4 values (D = measured in-situ concentration – equilibrium concentration at the time of sampling) were calculated in two ways (i) using in-situ measurements of atmospheric N_2O or CH_4 mole fractions when archived together with the dissolved concentration data in MEMENTO or (ii) using zonally averaged atmospheric N_2O and CH_4 mole fractions computed with the data from the World Data Centre for Greenhouse Gases (WDCGG, https://gaw.kishou.go.jp/) for the respective sampling month. N_2O and CH_4 flux densities were calculated by multiplying DN2O and DCH4 with the air-sea transfer coefficient (kw) which was estimated with the wind speed parameterization for kw from (Nightingale et al., 2000). Wind speeds for the respective sampling

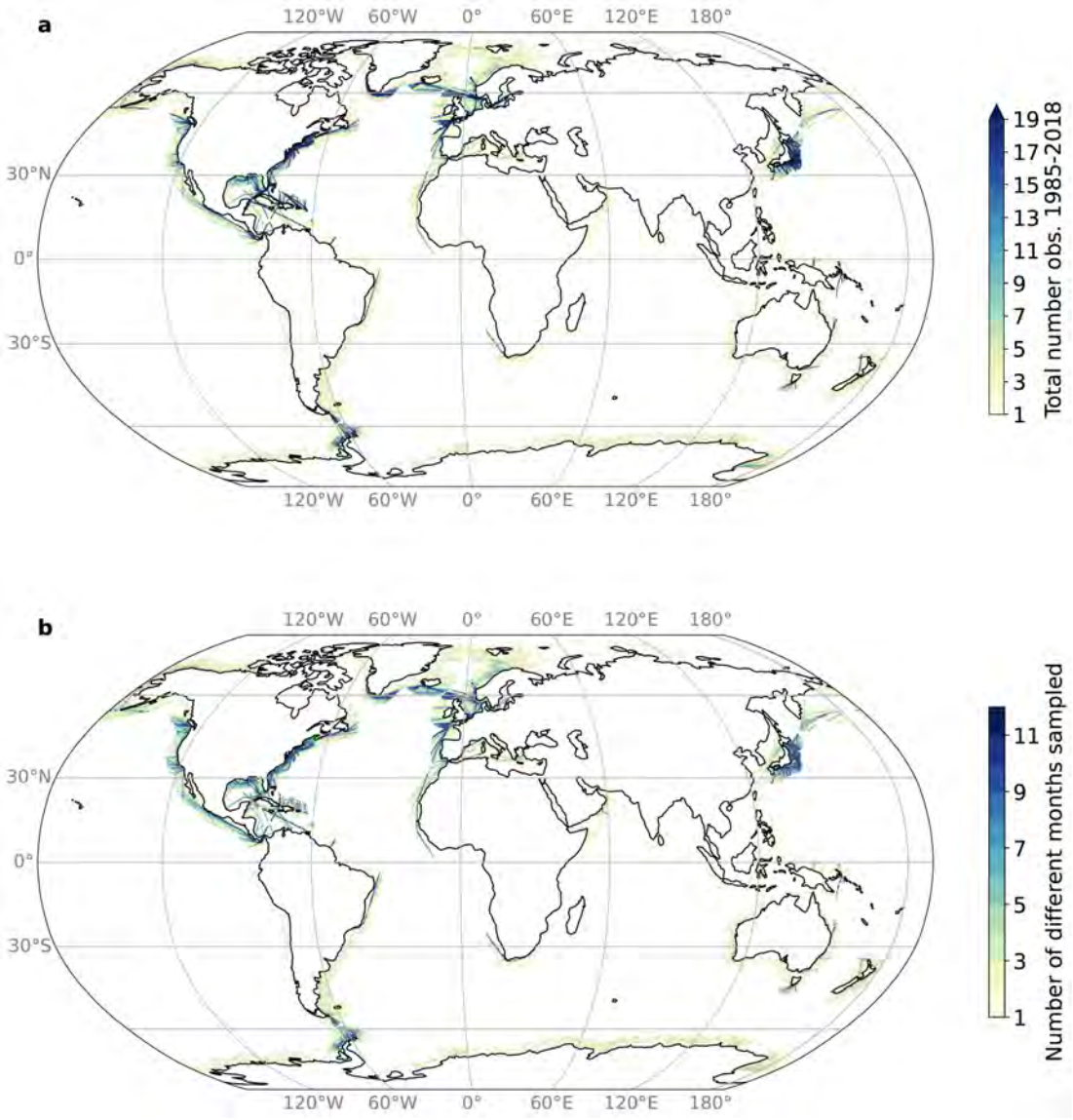

Figure S1. (a) areal coverage in 0.25 x 0.25 degree grid cells of SOCATv2.0 database calculated as the spatial density of the total number of observations 1985-2018 and (b) the number of distinct months sampled by SOCATv2.0 during this period. White areas represent where there are no observations (0 observations). See Methods and Laruelle et al. (2017) for definition of wide coastal ocean.

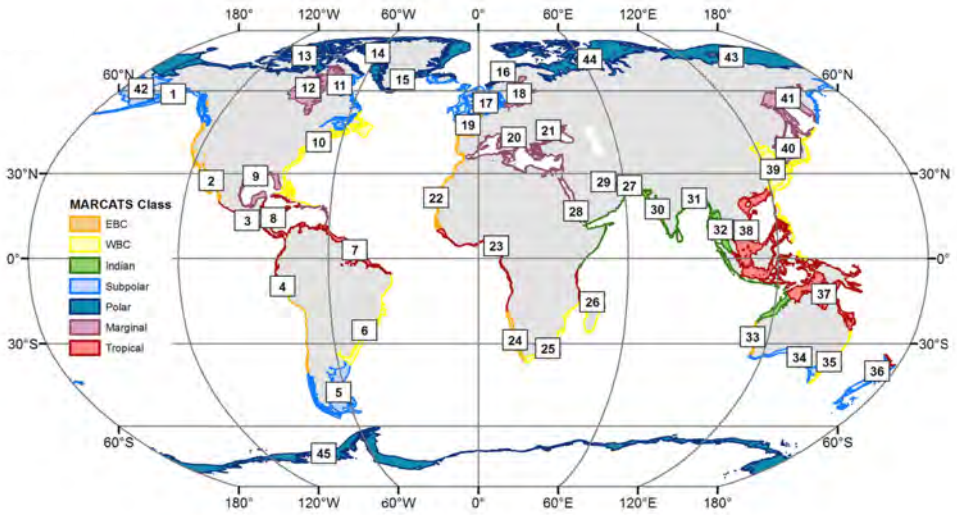

Figure S2. Locations of the 45 MARgins and CATchments Segmentation (MARCATS) regions (Laruelle et al., 2013) used to calculated the N_2O and CH_4 fluxes in MARCATS-N2O and MARCATS-CH4.

https://psl.noaa.gov) (Kanamitsu et al., 2002). Finally, the individual N_2O and CH_4 flux densities were averaged and extrapolated to the area of each MARCATS region to obtain an emission estimate for the individual MARCATS regions. The number of observatinos used in each MARCATS to derive the CH_4 and N_2O fluxes is listed in Table S1. MARCATS-N2O product has no observations in 6 MARCATS for the wide and 10 MARCATS for the narrow coastal oceans. Similarly, the MARCATS-CH4 has no observations in 8 MARCATS for the wide and 14 MARCATS for the narrow coastal oceans.

Yang-N2O

The N_2O air-sea flux reconstruction by Yang et al. (2020) is based on a synthesis of over 158,000 observations of N_2O mixing ratio, partial pressure, and concentration in the surface ocean from the MEMENTO database (Kock & Bange, 2015) and additional cruises (Yang et al., 2020). N_2O measurements are converted to surface N_2O mixing ratio anomalies using observations from the NOAA atmospheric flask dataset and extrapolated to a 0.25-degree resolution global monthly climatology using an ensemble of 100 random forest realizations. The random forest algorithm predicts N_2O mixing ratio anomalies based on their relationship to oceanographic predictors that include hydrographic variables, nutrients, oxygen, chlorophyll, net primary production, and seafloor depth. Reconstructed mixing ratio climatologies are used to estimate air-sea fluxes by applying a commonly used gas exchange parameterization (Wanninkhof, 2014). Two formulations of piston velocity are adopted: one based on a quadratic dependence on wind speed (Wanninkhof, 2014), and one that explicitly accounts for bubble-mediated fluxes (Liang et al., 2013). Sea ice cover, surface temperature, salinity and atmospheric pressure are taken from ERA5 reanalysis (Hersbach et al., 2020). Calculations are performed with two high-resolution wind products (ERA5 and Remote sensing Cross-Calibrated Multi-Platform version 2.0) that are available at 0.25, 6-hourly resolution for the period from 1988 to 2017, yielding four permutations of the piston velocity. The resulting ensemble of 400 global N_2O air–sea flux estimates is averaged in time to obtain monthly mean climatologies. A description of the dataset and methods is presented in (Yang et al., 2020). The compilation of N_2O measurements, the reconstructed global N_2O climatology and air-sea flux are available on the Biological and Chemical Oceanography Data Management Office (BCO-DMO) portal (DOI: 10.26008/1912/bco-dmo.810032.1). The code used to produce these datasets is archived on a public GitHub repository at https://github.com/yangsi7/mapping-ocean-n2o (DOI: 10.5281/zenodo.3757194).

Weber-CH4

The diffusive sea-air CH4 flux reconstruction by (Weber et al., 2019) is based on a compilation of 120,000 individual concentration and partial pressure measurements from the MEMENTO database (Kock & Bange, 2015) and additional cruise datasets (Weber et al., 2019). These measurements were converted to CH_4 disequilibrium using atmospheric partial pressure from the NOAA Global Monitoring Division archive, which has collected flask samples from a global network of monitoring stations since 1980 (www.esrl.noaa.gov/gmd/ccgg/) and extrapolated to a 0.25-degree monthly climatology using 10,000 artificial neural network and random regression forest models, each trained with 70% of the data. Air-sea fluxes were computed by combining each climatology with one of four piston velocity relationships (Wanninkhof, 1992, 2014; Nightingale et al., 2000; Liss & Merlivat, 1986), and one of four global wind products (ERA5, CCMP, NCEP, reanalysis products, and a blended WindSat/QuickSCAT satellite product). Flux calculations were conducted at daily resolution then integrated into an annual climatology representing the mean 1999-2016 flux. Ebullitive CH4 emissions to the atmosphere were estimated using literature ranges for the global ebullition rate from continental shelf sediments (Hornafius et al., 1999; Hovland et al., 1993) and a bubble transfer model to estimate the fraction of CH4 reaching the surface (McGinnis et al., 2006). Full methodology is described in Weber et al., 2019 and the product is available at https://figshare.com/articles/dataset/ocean_ch4_nc/9034451.

S1.c Global ocean biogeochemical models

CCSM-WHOI

The Community Earth System Model (CESM) is the global ocean component of a coupled climate/earth system model. The ocean component, the Biogeochemical Elemental Cycle (BEC) model, consists of an upper-ocean ecological module and a full-depth ocean biogeochemistry module both embedded in a three-dimensional (3-D) global physical ocean general circulation model. The physical model is the Parallel Ocean Program (POP) z-level, hydrostatic, primitive equation model. The specific CESM-LR version used here has coarse, non-eddy resolution and is described in detail in Doney et al. (2009). The ocean model is integrated in an uncoupled model forced with physical climate forcing from NCEP atmospheric reanalysis and satellite data products. The ecosystem module builds on traditional phytoplankton–zooplankton–detritus–nutrient food-web models and incorporates multi-nutrient limitation (N, P, Si, Fe) on phytoplankton growth and specific phytoplankton functional groups. The biogeochemical module includes full carbonate system thermodynamics and air–sea CO_2 and O2 fluxes, nitrogen fixation, denitrification and a dynamic iron cycle with atmospheric dust deposition, water-column scavenging and a continental sediment source. There are 14 main compartments: pico/nano-plankton, diatoms, and diazotrophs; zooplankton; suspended and sinking particulate detritus; and dissolved nitrate, ammonia, phosphorus, iron, silicate, oxygen, dissolved inorganic carbon, and alkalinity. The model was forced with the NCEP reanalysis and did not include nutrients or carbon inputs by rivers.

CNRM-LR and CNRM-HR

CNRM-LR and CNRM-HR are the Earth System Models of second generation developed by CNRM-CERFACS for the sixth phase of the Coupled Model Intercomparison Project (CMIP6). Their ocean component uses the Nucleus for European Models of the Ocean (NEMO) Version 3.6 (Madec et al., 2017) coupled to both the Global Experimental Leads and ice for ATmosphere and Ocean (GELATO) sea ice model (Salas Mélia, 2002) Version 6 and the marine biogeochemical model Pelagic Interaction Scheme for Carbon and Ecosystem Studies version 2-gas (PISCESv2-gas) (Aumont et al., 2015). In CNRM-LR, NEMOv3.6 operates on the eORCA1L75 grid, which offers a nominal resolution of 1 degree to which a latitudinal grid refinement of 1/3 degree is added in the tropics, while in CNRM-HR, NEMO is run on the eORCA025 grid having a 0.25 degree of horizontal resolution. Whatever the horizontal resolution, the ocean is described with 75 vertical layers using a vertical $z^\star$ coordinate with partial step bathymetry formulation (Bernard et al., 2006). The ocean layers are distributed unevenly as a function of depth with a resolution of 1 m at ocean surface to 200 m below 4000 m. Key differences between both configurations are detailed in Berthet et al. (2019). The simulations were forced at the surface by the atmospheric state of JRA55-do v1.5.0 (Tsujino et al., 2018). Atmospheric CO_2 concentration is given as annual means as specified by CMIP6 protocols and is linearly interpolated in time. Riverine inputs of dissolved inorganic carbon and alkalinity (Ludwig et al., 1996) as well as nutrients (Mayorga

Table S1. Number of observations and density [in observations per 10^6 km^2] from MEMENTO database used in each MARCATS to calculate the MARCATS-N2O and MARCATS-CH4 observational products in the wide and narrow coastals. See map in Figure S2 for MARCATS locations.

MARCATS	N_2O wide		N_2O narrow		CH_4 wide		CH_4 narrow	
	observations	density	observations	density	observations	density	observations	density
1	71	9	20	7	38	5	9	3
2	159	21	28	10	124	17	5	1
3	229	31	8	2	12	1	0	0
4	1301	179	551	204	20	2	13	4
5	248	34	129	47	26	3	15	5
6	539	74	148	54	4	0	1	0
7	375	51	250	92	4	0	0	0
8	136	18	0	0	0	0	0	0
9	0	0	0	0	1	0	0	0
10	575	79	411	152	0	0	0	0
11	259	35	0	0	2	0	0	0
12	0	0	0	0	0	0	0	0
13	130	17	130	48	117	16	102	37
14	28	3	7	2	13	1	7	2
15	472	65	70	25	28	3	0	0
16	519	71	330	122	28	3	3827	1420
17	1294	178	917	340	1013	139	1014	376
18	250	34	91	33	3312	457	15	5
19	457	63	481	178	629	86	648	240
20	102	14	39	14	111	15	52	19
21	3	0	4	1	32	4	24	8
22	1286	177	430	159	474	65	148	54
23	396	54	17	6	5	0	1	0
24	185	25	69	25	5	0	5	1
25	514	70	54	20	0	0	0	0
26	173	23	0	0	0	0	0	0
27	1306	180	6	2	557	76	1	0
28	0	0	0	0	0	0	0	0
29	0	0	0	0	0	0	0	0
30	243	33	47	17	16	2	1	0
31	289	39	22	8	55	7	62	23
32	321	44	21	7	20	2	24	8
33	476	65	76	28	7	0	0	0
34	88	12	20	7	53	7	12	4
35	276	38	206	76	113	15	144	53
36	144	19	16	5	43	5	10	3
37	37	5	37	13	7	0	3	1
38	182	25	129	47	89	12	46	17
39	253	34	111	41	72	9	48	17
40	0	0	0	0	0	0	0	0
41	0	0	0	0	22	3	3	1
42	62	8	48	17	17	2	13	4
43	33	4	17	6	659	90	655	243
44	48	6	0	0	85	11	36	13
45	1703	235	959	356	85	11	47	17

et al., 2010) are prescribed with a repeated seasonal cycle scaled on freshwater riverine inputs. Burial of carbon at the bottom of the ocean is emulated with a meta-model based on POC export (Aumont et al., 2015). Originally implemented by Martinez-Rey et al. (2015), the marine N_2O parameterization has benefited from a recoding and an improved calibration presented in Berthet et al. (2022). A comprehensive description of the configuration of the marine biogeochemical component is presented in Séférian et al. (2019).

FESOM-LR and FESOM-HR

We use the ocean circulation model FESOM1.4 (C. Wang et al., 2014) coupled to the ocean biogeochemical model REcoM2 (Hauck et al., 2020, 2013; Schourup-Kristensen et al., 2014). FESOM is an unstructured mesh model used in a low-resolution configuration (FESOM-LR) and a high-resolution configuration (FESOM-HR, see resolution meshes in Figure S3). The Regulated Ecosystem Model (REcoM) simulates the coupled cycles of carbon, nitrogen, silicic acid, iron and oxygen. In this version, it simulates two phytoplankton groups (small phytoplankton and diatoms) and one zooplankton group. It allows for variable stoichiometry in phytoplankton (C:N:Chl:CaCO3 for small phytoplankton and C:N:Chl:SI for diatoms), zooplankton (C:N) and detritus (C:N:Si). There are no inputs of carbon or nutrients by rivers and runoff. The FESOM-LR configuration is based on a coarse mesh with a global nominal resolution of 1 degree, which is increased to about 25 km north of 50°N and to about 1/3° in the equatorial belt, and is also moderately refined along the coasts (Sein et al., 2018). The model is started from initial conditions (World Ocean Atlas for nutrient fields (Garcia et al., 2014), Glodap for alkalinity and preindustrial dissolved inorganic carbon (Lauvset et al., 2016)). It is spun up from 1850-1957 years using repeated year atmospheric forcing from the year 1961. The atmospheric forcing fields for the spin-up and for the simulation period 1958 to 2018 are taken from the Japanese 55-year Reanalysis Version 1.4.0 (Tsujino et al., 2018). Further, spin-up and simulation period are forced with observed atmospheric CO_2 as provided by the Global Carbon Budget (Friedlingstein et al., 2020). Carbonate chemistry and air-sea CO_2 exchange are calculated with the mocsy routines (Orr et al., 2015) that apply a quadratic gas-exchange parameterization (Wanninkhof, 2014). This is the same model version as used in the Global Carbon Budget 2020

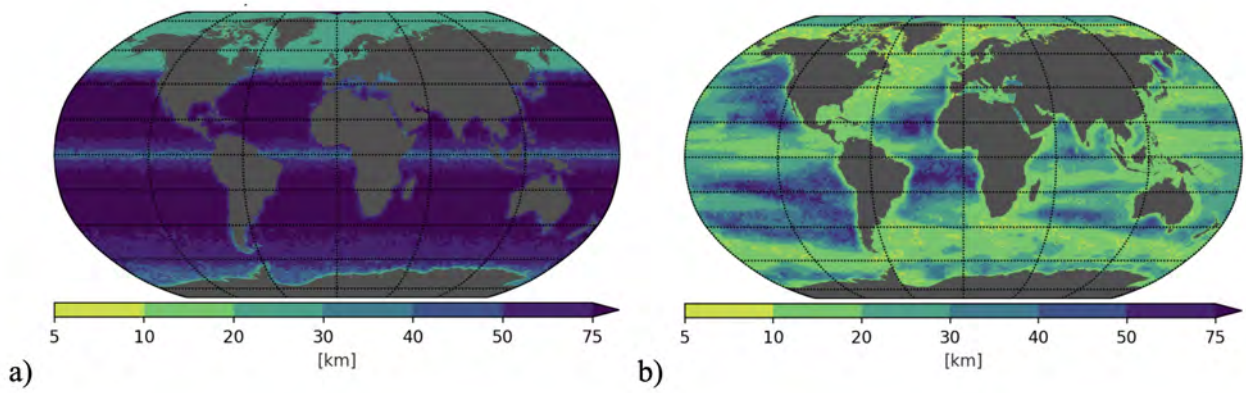

Figure S3. Horizontal resolution of the a) FESOM-LR and b) FESOM-HR models.

(Friedlingstein et al., 2020). The FESOM-HR configuration has a locally eddy-resolving mesh with the horizontal resolution varying according to the observed sea surface height (SSH) variability. The coarsest resolution is 60 km, and the finest is 8-10 km (Sein et al., 2018). This is equivalent to a 1/10° – 1/4° resolution. In particular, the high resolution is located along the pathways of the main currents, including the Gulf Stream. We performed a high-resolution physical ocean model spin-up run under JRA55 forcing. The spin-up spanned one full cycle from 1958-2017, and a second cycle 1958-1980 using FESOM-HR. We initialized our model from an existing simulation driven by CORE-II forcing (Large & Yeager, 2009). We branched off our simulations with coupled physics and biogeochemistry at the end of 1980 and ran the simulation from 1981 to 2019 using the HR mesh with an increasing atmospheric CO_2 concentration and interannual varying atmospheric forcing. The initial biogeochemical model fields for the year 1980 are taken from the FESOM-LR simulation and are interpolated to the FESOM-HR mesh.

IPSL

The IPSL ocean model uses the Nucleus for European Models of the Ocean (NEMO) Version 3.6 which includes three components, ocean physics from NEMO-OPA (Madec et al., 2017), the sea ice dynamics and thermodynamics from NEMO-LIM3 (Rousset et al., 2015), and the ocean biogeochemistry from NEMO-PISCES-v2 (Aumont et al., 2015). The global configuration used here is eORCA1L75, including a horizontal nominal resolution of 1° (with a latitudinal grid refinement of up to 0.3° in the equatorial region) and 75 levels on the vertical (with the partial step formulation of Barnier et al. (2006) and layer thicknesses increasing from 1m at the surface to 200m at the bottom). The simulation is forced at the surface by the atmospheric reanalysis product of JRA55-do-v1.4 (Tsujino et al., 2018) and global and annual mean values of atmospheric CO_2 as specified in the Global Carbon Budget protocol (Friedlingstein et al., 2022). Riverine inputs of carbon, alkalinity and nutrients are based on (Ludwig et al., 1996) and (Mayorga et al., 2010), and prescribed with a repeated seasonal cycle. Sediment burial of carbon, alkalinity and nutrients is simulated using the formulation of (Dunne et al., 2007) and (Middelburg et al., 1996).

MOM6-Princeton

The MOM6-Princeton model uses the Modular Ocean Model version 6 (MOM6), the Sea Ice Simulator version 2 (SIS2), and the Carbon Ocean Biogeochemistry and Lower Trophics version 2 (COBALT v2) developed by the NOAA Geophysical Fluid Dynamics Laboratory (GFDL). The specific version used here is available on Github (Git commit: 48536b downloaded in October 2018) and was used in Liao et al. (2020) and the global carbon budget 2020 (Friedlingstein et al., 2020). The physical and biogeochemical ocean configurations follow GFDL earth system model version 4 (ESM4) (Dunne et al., 2020)). The horizontal resolution is 0.5° in longitude and 0.25-0.5° in latitude. On the vertical, it includes 75 hybrid isopycnal $z^\star$ coordinate, including a $z^\star$ coordinate near the surface (about 2 m thick layers in the upper 20 m in the tropical Pacific Ocean) and a modified potential density coordinate below (Adcroft et al., 2019). COBALT2 includes 33 state variables, including nutrients (nitrate, phosphate, and iron), silicate, three phytoplankton groups, three zooplankton groups, three dissolved organic carbon pools, one particulate detritus pool, oxygen, and the carbonate system (Stock et al., 2020). The model was spun up from rest for 81 years by repeating the year 1959 of the JRA55-do v1.3 forcing. Temperature, salinity, nutrients (nitrate, phosphate, and silicate), and oxygen were initialized from World Ocean Atlas version 2013 (Garcia et al., 2014; Locarnini et al., 2014; Zweng et al., 2014). Initial dissolved inorganic carbon (DIC) and alkalinity (Alk) are from GLODAP v2 (Olsen et al., 2016). The initial DIC is corrected for the accumulation of anthropogenic carbon to match the level expected in 1959 using the data-based estimate of ocean anthropogenic carbon content (Khatiwala et al., 2013). Other COBALT tracer initial conditions (e.g., ammonium, calcium carbonate) are from a preindustrial GFDL-ESM2M-COBALT simulation (Stock et al., 2014). The simulation includes riverine nutrients from the GlobalNEWS2 model (Mayorga et al., 2010) and riverine carbon inputs designed to roughly balance carbon burial in the model (here input of 0.11 of DIC and 0.07 of DOC). At the end of the 81-year spin-up, the model has reached a near-equilibrium between atmospheric pCO_2 and surface ocean pCO_2 , with a drift in global air-sea CO_2 flux ¡0.004 PgC/yr over the last 10 years of spin-up. The simulation was then performed from 1959 to 2018 using interannual forcing. In this version, the gas transfer coefficient was calculated using the parameterization of (Wanninkhof, 1992) but with the updated Schmidt number from (Wanninkhof, 2014).

MPIOM-HAMOCC

The Hamburg Ocean Carbon Cycle (HAMOCC) (Ilyina et al., 2013; Paulsen et al., 2017) model is a global ocean biogeochemical model embedded in the Max Planck Institute Ocean Model (MPIOM) (Jungclaus et al., 2013). The version used here is the same as used in the Global Carbon Budget 2021 (Friedlingstein et al., 2022). The nominal resolution here is 1.5 degree with 40 vertical levels.

The biogeochemical cycles of carbon, nutrients (nitrate, phosphate, iron), oxygen, silicate, phytoplankton (bulk and cyanobacteria), zooplankton, detritus, and organic matter in HAMOCC are computed in the water column and in the upper sediment. Biogeochemical tracers are transported with the ocean flow in the same way as temperature and salinity in MPIOM. The composition of organic matter follows a constant Redfield ratio of carbon (C:N:P:O2 = 122:16:1:-172). The sinking of organic matter follows the Martin curve, i.e. linearly increasing with depth. River inputs of carbon and nutrients are included (Lacroix et al., 2021). NCEP 6 hourly cyclic forcing (10 years starting from 1948) is used for the spin-up, transient NCEP forcing has been used during 1948- 2021.The air-sea gas exchange parameterization follows the OMIP protocol (Orr et al., 2017).

MRI-ESM2-1

MRI-ESM2-1 is a modified version for the ocean component of Meteorological Research Institute Earth System Model version 2 (MRI-ESM2) (Yukimoto et al., 2019). The source code is taken from Meteorological Research Institute Community Ocean Model version 4 (MRI.COMv4) (Tsujino et al., 2017), which is formulated on general orthogonal curvilinear coordinate in the horizontal and $z^\star$ coordinate in the vertical directions and is discretized on Arakawa B-grid frame. The horizontal resolution is 1.0° in the zonal and 0.3–0.5° in the meridional directions. There are 60 vertical levels with enhancement in the upper layer and an additional bottom boundary layer at the seafloor in the deep and bottom water formation regions such as the northern North Atlantic and in the Southern Ocean around Antarctica. The configuration and performance of this model in terms of physical fields are fully described and presented by Urakawa et al. (2020). The biogeochemical processes consist of a carbon cycle model with the carbonate chemistry and the surface gas exchange parameterization that follow the protocols of OMIP-BGC (Orr et al., 2017) and a simple NPZD (nutrient, phytoplankton, zooplankton, detritus) type ocean ecosystem model as used by (Nakano et al., 2011). Relative to the version used for CMIP6 (MRI-ESM2-0), the sinking velocity of detritus is changed from 7.0 m day-1 to 2.0 m day-1. Advection scheme for biogeochemical tracers is changed from MPDATA (Multi-dimensional Positive Definite Advection Tracer Algorism) to PPM (Piecewise Parabolic Method). The simulation was forced at the surface by the atmospheric state of JRA55-do v1.5.0 (Tsujino et al., 2018). Atmospheric CO_2 concentration is given as the spatially uniform, annual mean as specified by CMIP6 protocols and is linearly interpolated in time. No riverine inputs of nutrients or carbon and no burial are included. Instead, surface DIC and Alkalinity fluxes are added in proportion to surface salinity flux due to a restoring of the model sea surface salinity to that of World Ocean Atlas 2013 version 2 (WOA13v2).

NEMO-PlankTOM

The NEMO-PlankTOM model is based on the ORCA2 version of the NEMO physical model, which calculates vertical diffusion explicitly and includes a dynamic-thermodynamic sea-ice model. PlankTOM is the biogeochemical module that represents full cycles of carbon, oxygen, phosphorus, silica, calcite, and a simplified cycle for iron and nitrogen. PlankTOM12, used here for its estimate of CO_2 fluxes, represents twelve Plankton Functional Types, six phytoplankton, five zooplankton and archaea. The version used here is based on the work of (Wright et al., 2021) and integrates pteropods and the aragonite cycle from (Buitenhuis et al., 2019). This is the same version published in the Global Carbon Budget 2022 (Friedlingstein et al., 2022). The model is initialized in 1750 and run forward with constant atmospheric forcing up to 1948, then forced with daily weather conditions using the NCEP reanalysis data, and constant input of nutrient (N, P and Fe) and organic and inorganic carbon from rivers (see also Friedlingstein et al. 2022). NCEP winds are also used to calculate the gas exchange velocity using (Wanninkhof, 1992) formulation. PlankTOM5 is used to estimate N_2O fluxes. PlankTOM5 uses a simplified ecosystem composition with three phytoplankton and two zooplankton, and a full representation of N_2O production and loss processes (Buitenhuis et al., 2018).

NorESM-OC2.0

NorESM-OC2.0 is the ocean carbon-cycle stand-alone configuration of the Norwegian Earth System Model version 2 (NorESM2, (Seland et al., 2020; Tjiputra et al., 2020). The physical ocean component of NorESM2, the Bergen Layered Ocean Model (BLOM), is configured on a tripolar grid with a nominal resolution of 1° horizontally and 51 isopycnic layers in the vertical with 2 additional layers representing a bulk mixed layer on top. Ocean biogeochemistry is represented by the iHAMOCC model, which is derived from HAMOCC5 (Ilyina et al., 2013) and includes a 12-layer sediment scheme. The iHAMOCC model includes a NPZD ecosystem parameterization (Six & Maier-Reimer, 1996) and carbon chemistry follows the OCMIP protocols (Orr et al., 2015). The influx of carbon and nutrients from rivers to the coastal oceans has been implemented based on the Global-NEWS2 model (Mayorga et al., 2010) and work by (Hartmann et al., 2009) for DIC and alkalinity fluxes. Riverine fluxes are distributed as a function of river mouth distance (with an e-folding length scale of 1000 km and cutoff of 300 km) to the ocean grid and are assumed to be constant over time at year 2000 levels. The NorESM-OC2.0 simulation used here follows the CMIP6 omip2 protocol, which employs the JRA-55 atmospheric forcing data set. The gas exchange coefficient formulation is from (Wanninkhof, 2014).

ECCO2-Darwin and ECCO-Darwin

Global air-sea fluxes of N_2O were evaluated from two versions of the ECCO family: the ECCO2-Darwin and ECCO-Darwin models which include the same biogeochemical component Darwin but are embedded in two different ocean physical settings. ECCO2-Darwin model, is a global physical-biogeochemical ocean model with nominal horizontal grid of 1/6 of degree therefore eddy-permitting at lower latitudes. It is forced with ECMWF winds over the 2006-2008 period and JRA-55 winds over the 2009-2013 period, optimized with adjoint technique in order to realistically represent the observed physical ocean climate variability. ECCO-Darwin, a global physical-biogeochemical ocean model with nominal horizontal grid resolution of 1/3 of degree, and is forced with ERA-Interim winds (Carroll et al., 2020). Both models have 50 vertical levels and in the top 100 m the model is vertically resolved with 10-meter grid boxes. An extensive description of this model run of ECCO2-Darwin including the optimized atmospheric forcing spanning from 2004 to 2013 can be found in (Manizza et al., 2019) while for ECCO-Darwin a more detailed model description can be found in Carroll et al. (2020). The Darwin biogeochemical/ecological model used for this study explicitly represents the cycle of carbon, oxygen, phosphorus, silica, and iron in the global ocean. It also has an ecosystem component representing five groups of phytoplankton and two groups of zooplankton (Manizza et al., 2019; Carroll et al., 2020). For this particular version of the model we implemented a parameterization of the oceanic cycle of (Manizza et al., 2012) using the scheme of (Nevison et al., 2003) based on the oceanic oxygen cycle previously represented in ECCO2-Darwin model (Ganesan et al., 2020). The air-sea gas flux of N_2O was parameterized according to Wanninkhof (1992). In addition, a thermal-only N_2O

tracer (a tracer in which biogeochemical sources and sinks are suppressed but with the same solubility as N_2O) was also added to the model to isolate the process of ocean ventilation affecting the N_2O concentration in the ocean at seasonal time scales as done in (Manizza et al., 2012). The ventilation component of the air-sea N_2O fluxes is obtained by subtracting the solubility-only N_2O air-sea flux from the total N_2O air-sea flux. In the ECCO2-Darwin simulation the 2004-2005 period was discarded and we used the 2006-2013 period only for our analysis. However, the ECCO-Darwin numerical simulation was run for the 1992-2014 period but we discarded the inclusion of the output relative to the 1992-1996 period in our analysis due to the model adjustment in this initial part of our numerical simulation.

S1.d Regional ocean biogeochemical models

ACM-NWAtl

The model is based on the Rutgers version of the Regional Ocean Modelling System (ROMS) (Haidvogel et al., 2008), has 30 vertical levels and approximately 10 km horizontal resolution (240×120 horizontal grid cells). The model uses atmospheric surface forcing from the European Centre for Medium-Range Weather Forecasts (ECMWF) global atmospheric reanalysis (ERA-Interim) (Dee et al., 2011), and CO_2 fluxes are calculated following the Ho et al. (2006) parameterization. Within the ocean, it uses the GLS vertical mixing scheme (Umlauf & Burchard, 2003; Warner et al., 2005), and the "high-order spatial interpolation at the middle temporal level" (HSIMT) advection scheme for tracers (Wu & Zhu, 2010). Physical initial and boundary conditions are defined using the regional physical ocean model of the northwest North Atlantic by Urrego-Blanco and Sheng (2012). Climatological river discharge is imposed for 12 major rivers and uses observed long-term monthly means from the Water Survey of Canada. Full details on the physical model setup and its validation can be found in Brennan et al. (2016) and Rutherford and Fennel (2018). These studies have shown that the model simulates the vertical structure and seasonal variations of temperature and salinity on the shelf well. The model captures mesoscale features and coastal upwelling events and simulates the volume transport throughout the region in agreement with observation-based estimates.

The biogeochemical model is based on the nitrogen-cycle model with the inorganic carbon component of (Fennel et al., 2006) and Fennel and Wilkin (2009) but was recently expanded to include two phytoplankton and two zooplankton functional groups (Laurent et al., 2021). For a detailed description and validation of the biological model and the model's carbonate system parameters, we refer to Laurent et al. (2021) and Rutherford et al. (2021) respectively. Laurent et al. (2021) compared the model output with glider transects of temperature, salinity, and chlorophyll and in situ measurements of chlorophyll and nitrate. Rutherford et al. (2021) compared models results against a high-resolution pCO_2 time series and frequent cross-shelf transects of pCO_2 to ensure it faithfully represents both the seasonal cycle and cross-shelf gradients. Atmospheric pCO_2 is set to the seasonal cycle and secular trend derived from Sable Island monitoring data contributed by Environment Canada's Greenhouse Gas Measurement Program (Environment and Climate Change Canada: Canadian Greenhouse Gas Measurement Program). The long-term linear trend in the atmospheric pCO_2 is $\sim$2 uatm yr^{-1}. Further details of the biogeochemical model, including the carbonate chemistry equations, can be found in the supplementary information of (Laurent et al., 2017). Nitrate concentrations in rivers are prescribed from Global NEWS model output (Seitzinger et al., 2005). DIC and total alkalinity (TA) in rivers were calculated by fitting a linear relationship with salinity from Gulf of St. Lawrence bottle data and extrapolating to river water salinity.

ROMS-ETHZ-Atl and ROMS-ETHZ-Pac

The two regional models ETHZ-ROMS-Pac and ETHZ-ROMS-Atl rely on the coupling of the Regional Oceanic Modeling System (ROMS) (Shchepetkin & McWilliams, 2005) with the biogeochemical/ecological model BEC (Moore et al., 2013). Both setups rely on a telescopic grid that permits the model to resolve the mesoscale coastal processes in the region of interest, while covering at the same time nearly the entire ocean basin. In the ETHZ-ROMS-Pac setup, the telescopic grid is centered on the US West coast (resolution 4km), while in the ETHZ-ROMS-Atl setup, the telescopic grid has two poles, one centered in the Amazon outflow region (resolution 4km), and one on Western Africa. BEC simulates the cycling of carbon and 4 nutrients (N, P, Si, Fe) which govern, along with light and temperature, the growth of three phytoplankton types (Small Phytoplankton, Diatoms and Trichodesmium). The ETHZ-ROMS-Atl setup includes a fourth phytoplankton type representing a symbiosis between a diatom and a N2-fixer, i.e., Diatom-Diazotroph-Assemblages that have been shown to be regionally important for the cycling of carbon (Louchard et al., 2021). All phytoplankton are grazed by one zooplankton class. Particulate organic matter (POM) is produced as a result of non-grazing mortality, aggregation or grazing processes. POM is then exported and remineralized in an explicit manner (Frischknecht, 2018) in ETHZ-ROMS-Pac and following an implicit scheme in ETHZ-ROMS-Atl (Armstrong et al., 2001). The atmospheric forcing of surface short and long-wave radiations, wind stress, and surface freshwater fluxes is derived from the hourly ERA5 regridded product from 1979 to 2019 (Copernicus Climate Change Service [C3S], 2017; (Hersbach et al., 2020)). Additionally, the atmospheric forcing includes monthly varying atmospheric pCO_2 provided by (Landschützer et al., 2020), considering the dry air mixing ratio for the marine boundary layer from GLOBALVIEW-CO2 (2014), the atmospheric pressure and the water vapor contribution from Dickson et al. (2007). Also included in the atmospheric forcing are the input of iron from dust and nitrogen deposition, and only in the ETHZ-ROMS-Atl setup, phosphorus deposition, all derived from (Mahowald et al., 2009). The initial conditions and the boundary conditions are based on World Ocean Atlas for the main nutrients (Garcia et al., 2014). For DIC and Alkanity, GLODAP gridded products (Global Ocean Data Analysis Project version 2, (Lauvset et al., 2016)) are used as a climatology (centered on 2002) in ETHZ-ROMS-Alt and to create transiently evolving conditions in ETHZ-ROMS-Pac, following the procedures described by (Franco et al., 2018). Major rivers in the domain are represented as a surface flux of freshwater and nutrients (N,P) as described in (Frischknecht, 2018). One exception in the ETHZ-ROMS-Atl setup is the Amazon River that is represented by an inflow across an open lateral boundary condition and is delivering the whole suite of dissolved inorganic/organic nutrients and dissolved organic/inorganic carbon (estimates based on (Araujo et al., 2014)).

ROMS-NYUAD-Indian

The circulation model is based on the Regional Ocean Modeling System (ROMS) (Shchepetkin & McWilliams, 2005). Vertical mixing is represented using the non-local K-profile parameterization (KPP) scheme (Large et al., 1994). The model domain covers the Indian Ocean from 31.5S to 31N and 30E to 120E with a 1/10 degree horizontal resolution and 32 sigma-coordinate vertical layers with refined resolution near the surface. Coupled to the hydrodynamic model is a nitrogen-based nutrient, phytoplankton zooplankton, detritus (NPZD) model with two components for nutrients, nitrate and ammonium, one phytoplankton, one zooplankton, and two detrital classes (Gruber

et al., 2006). The model has a module describing the cycling of oxygen as well as a parameterization of water column and benthic denitrification (Lachkar et al., 2016, 2021). The model also includes a carbon module with three state variables: DIC, Total Alkalinity, and calcium carbonate (Gruber et al., 2012; Lachkar & Gruber, 2013; de Verneil et al., 2022). Organic carbon is linked to organic nitrogen through the Redfield ratio 106:16. Surface fluxes of DIC and Total Alkalinity driven by changes in sea surface salinity are included as virtual fluxes proportional to the sea surface salinity forcing. Carbonate chemistry is calculated using routines from the Ocean Carbon-Cycle Model Intercomparison Project (OCMIP) (Orr et al., 2005). The formulation of air-sea gas transfer uses a quadratic wind speed dependence following Wanninkhof (1992). Further details of the biogeochemical model are provided in (Lachkar et al., 2021; de Verneil et al., 2022). The hindcast simulation is forced with ECMWF ERA-Interim 6-hourly heat fluxes, air temperature, pressure, humidity, precipitation and winds over the period from January 1980 to December 2018. Initial and lateral boundary conditions for temperature, salinity, currents and sea surface height are based on the ECMWF Ocean Reanalysis System 5 (ORAS5). The initial and lateral boundary conditions for nitrate and oxygen are extracted from the World Ocean Atlas 2018. The initial and lateral boundary conditions for DIC and alkalinity are based on GLODAP. Atmospheric CO_2 concentrations are prescribed from monthly Mona Loa data (Keeling et al., 2005). Riverine inputs include nutrients (Krishna et al., 2016; Ramesh et al., 1995) but no carbon or alkalinity. To account for the accumulation of anthropogenic carbon at the lateral boundaries during the simulation period, we used decadally-varying DIC based on available estimates of anthropogenic CO_2 (Key et al., 2004; Gruber et al., 2019; Olsen et al., 2019) regressed to atmospheric CO_2 concentrations. Initial and boundary conditions for DIC and alkalinity are processed following de Verneil et al. (2022) to include a seasonal cycle in the upper ocean. The model is spun up for 30 years with a repeated normal year (1984) forcing. During the spin-up phase (1950-1979), time-varying atmospheric CO_2 concentrations and DIC are prescribed at the atmospheric and lateral boundaries, respectively. Atmospheric CO_2 data prior to 1958 is based on (Joos & Spahni, 2008).

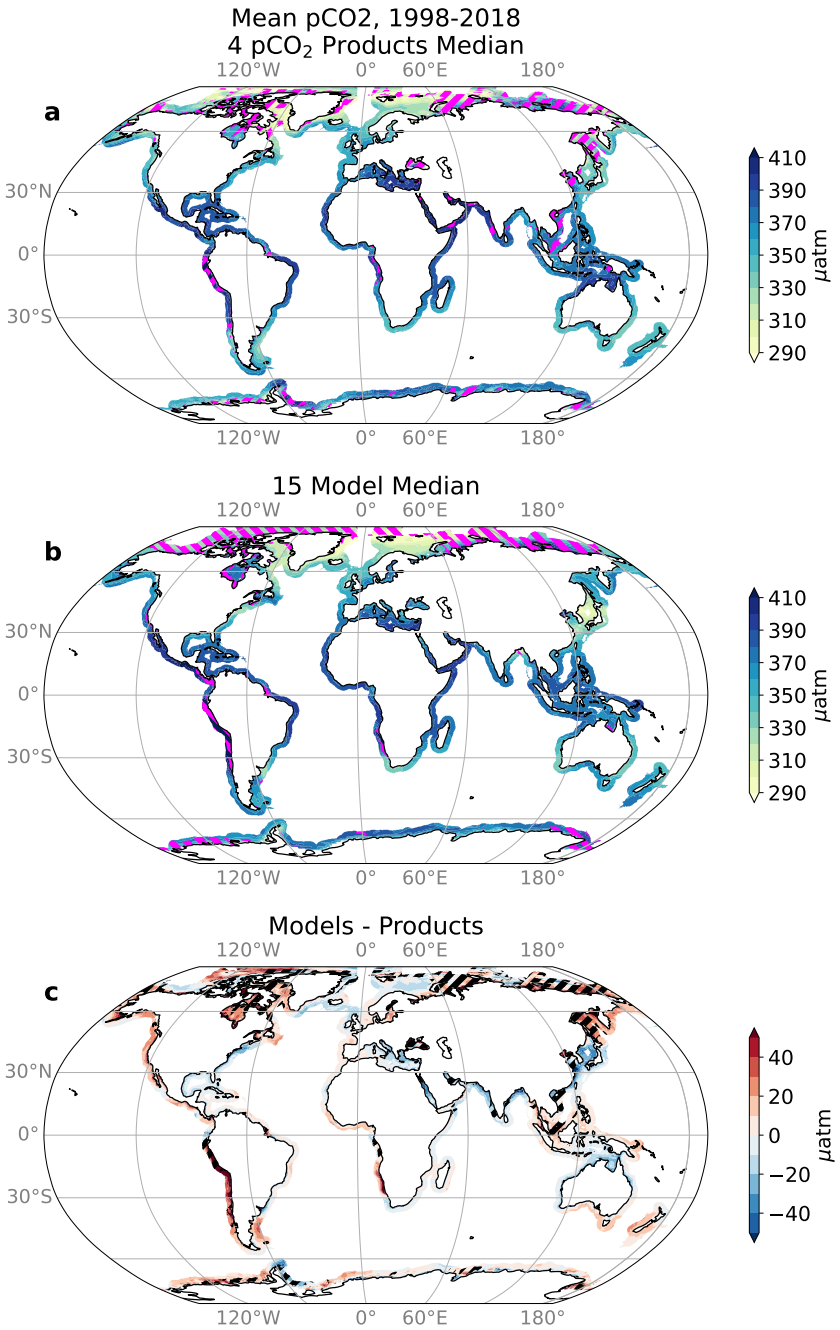

Figure S4. Annual mean coastal pCO_2 (in wide coastal ocean) for a) the 4-product median, b) the 15-model median, and c) the difference between model and product medians. The model median in each point is calculated using the 11 global models and the 4 regional models. All are for 1998-2018 except coastal-SOM-FFN and merged-SOM-FFN pCO_2 products available for 1998-2015 only. Hatching indicates the coastal area with RMSD greater than 25 uatm across pCO_2 products (panels a and c) or 33 uatm across models (panel b) (20% of coastal area with highest RMSD in each case). Here pCO_2 is masked where sea ice on average covers 50% of the grid cell, to improve visual comparison with the flux.

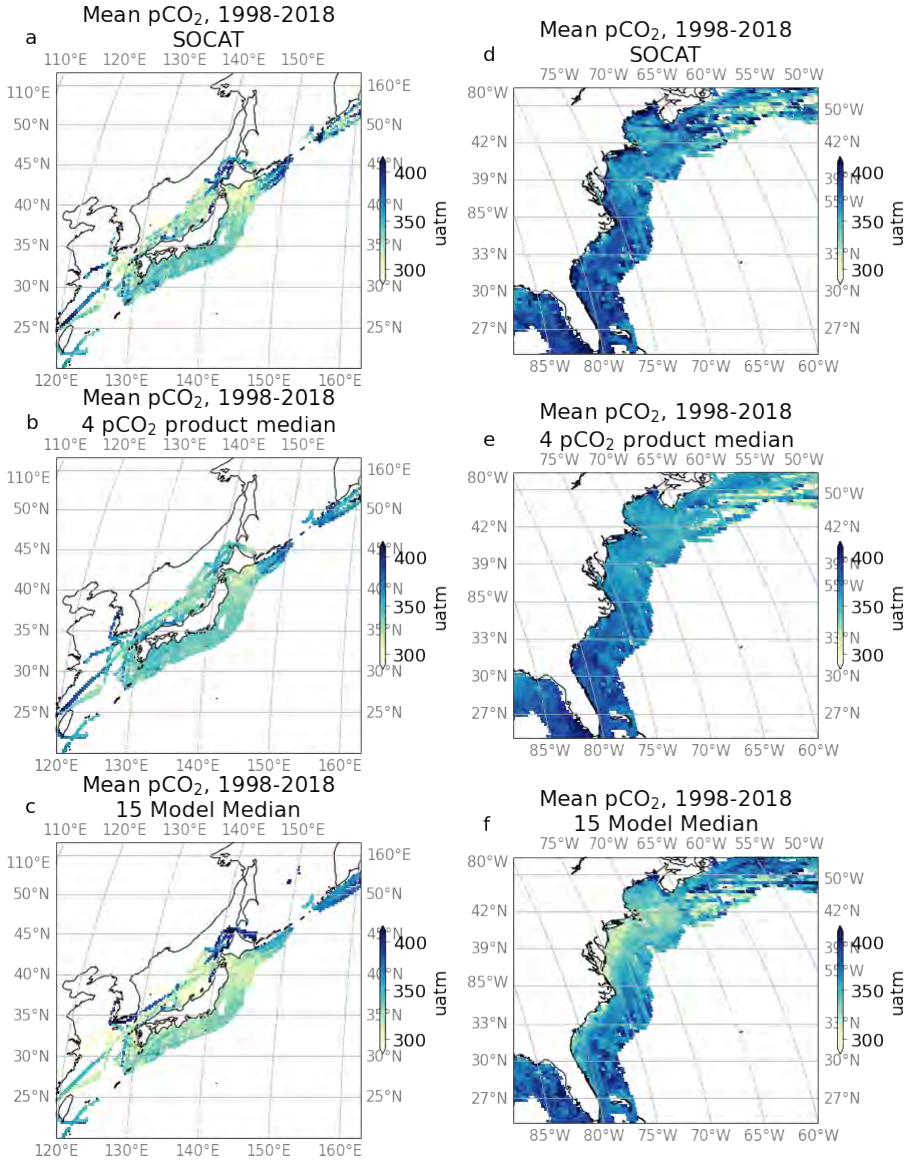

Figure S5. Mean coastal pCO_2 (in wide coastal ocean) for the SOCAT pCO_2 dataset (top row), the 4-product median (middle row), and the 15-model median (bottom row) along the coast of Japan (left column) and the eastern US (right column). The model median in each point is calculated using the 11 global models and the 4 regional models. Subsampling was done by sampling monthly climatologies of each products and models at the location and month of the SOCAT observations.

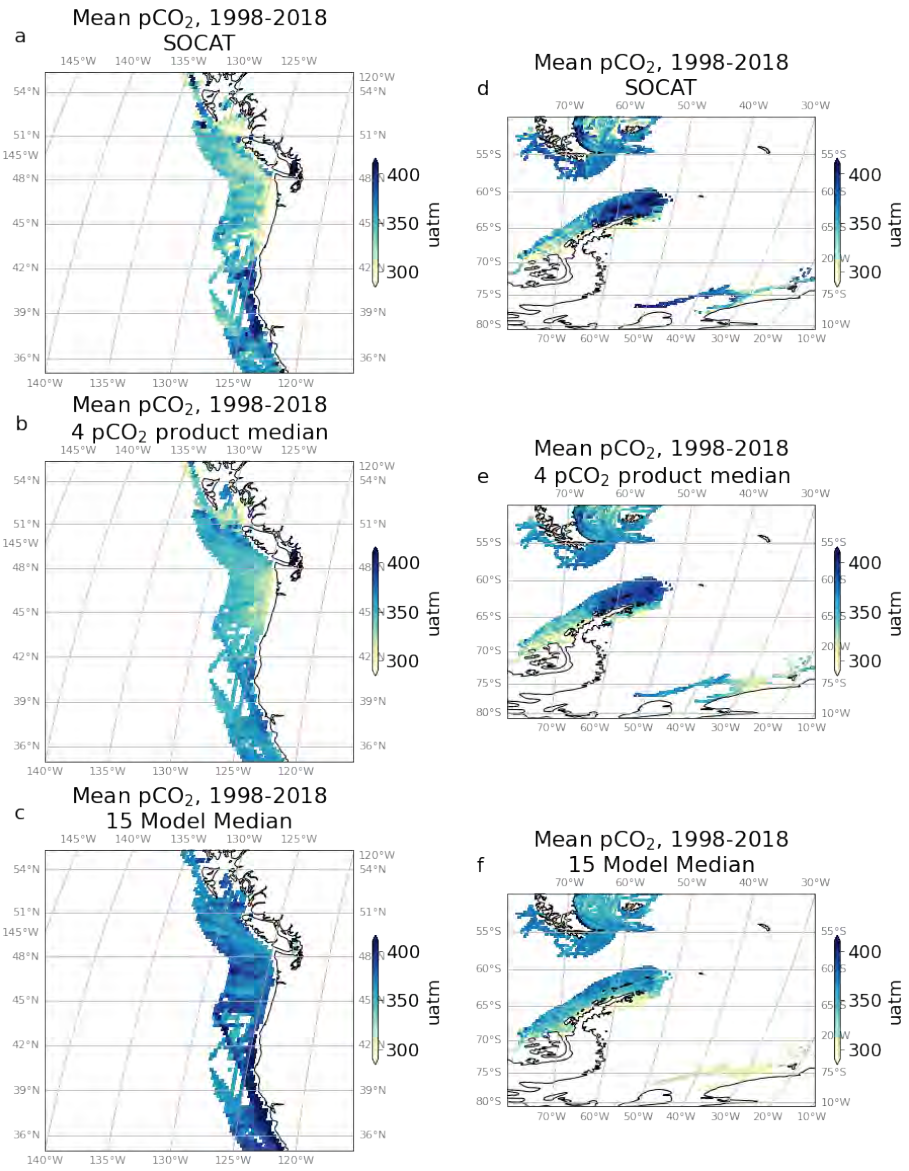

Figure S6. Mean coastal pCO_2 (in wide coastal ocean) for the SOCAT pCO_2 dataset (top row), the subsampled 4-product median (middle row), and subsampled 15-model median (bottom row) along the coast of the Antarctic Peninsula (left column) and the Peruvian margin (right column). The model median in each point is calculated using the 11 global models and the 4 regional models. Subsampling was done by sampling monthly climatologies of each products and models at the location and month of the SOCAT observations.

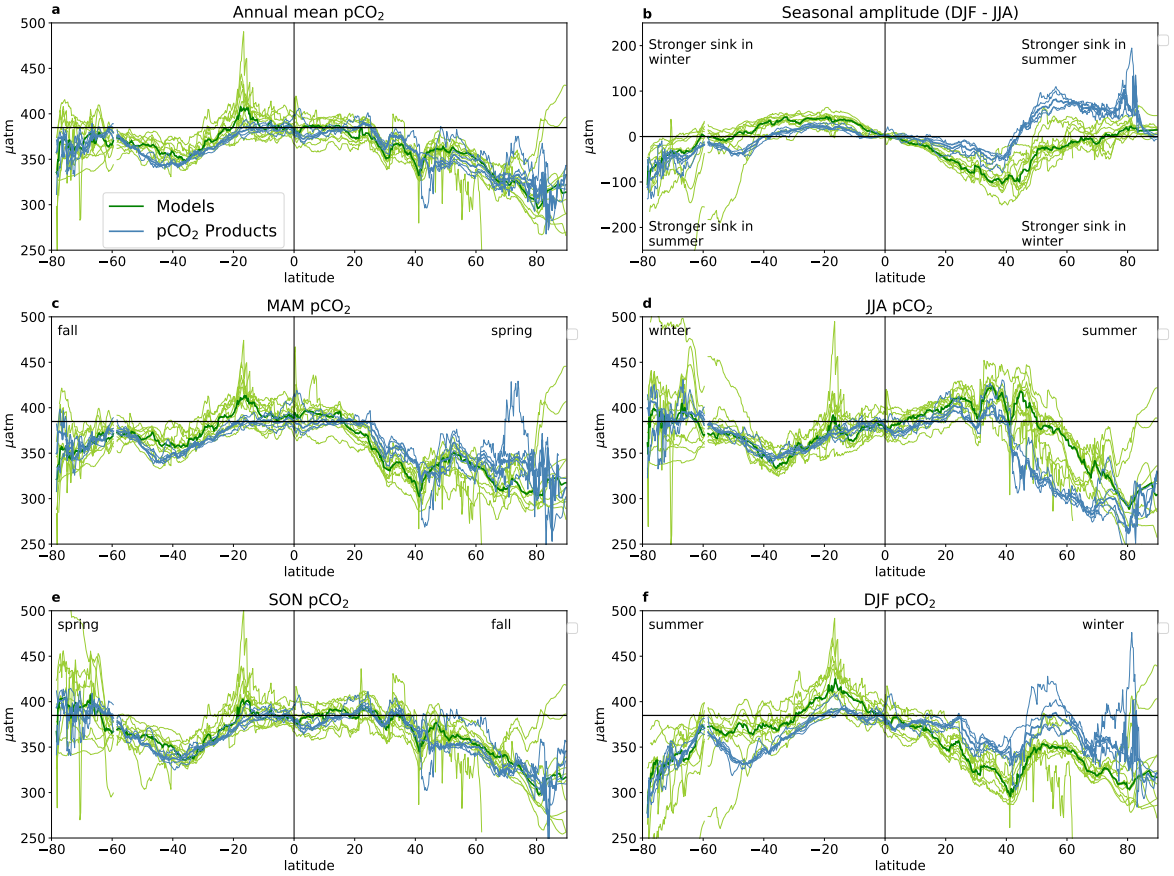

Figure S7. Latitudinal distribution of wide coastal ocean a) annual mean pCO_2, b) pCO_2 seasonal amplitude computed as December-February minus June-August, c) March-May pCO_2, d) June-August pCO_2 , e) September-November pCO_2, and f) December-February pCO_2 for the product and model medians (thick lines). Thin lines indicate the mean pCO_2 in each of 11 global models (green) and the 4 products (blue).

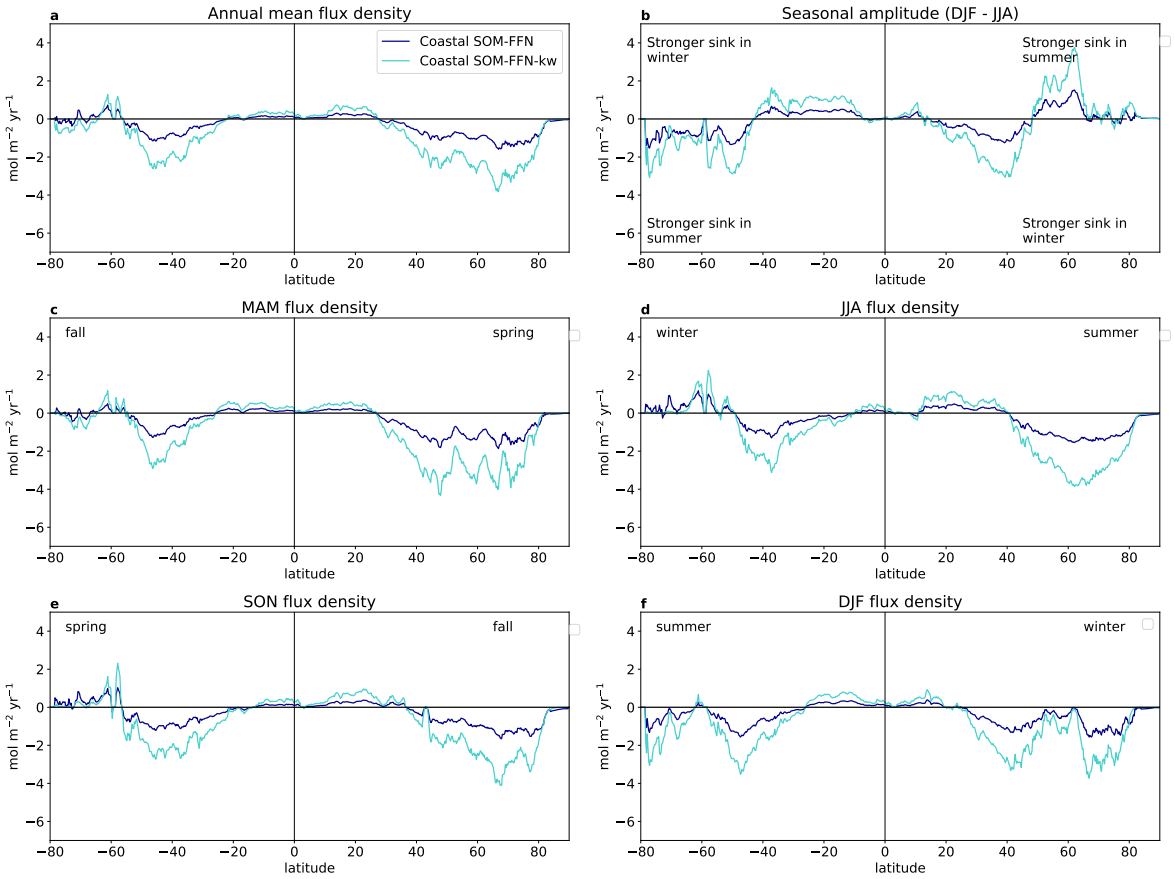

Figure S8. Influence of wind speed and gas exchange coefficient. Latitudinal distribution of coastal ocean (wide shelf) a) annual mean CO_2 flux, b) CO_2 flux seasonal amplitude computed as December-February minus June-August, c) March-May CO_2 flux, d) June-August CO_2 flux, e) September-November CO_2 flux, and f) December-February CO_2 flux in Coastal-SOM-FFN and Coastal SOM-FFN-kw (different wind product and gas exchange coefficient formulation, see Methods).

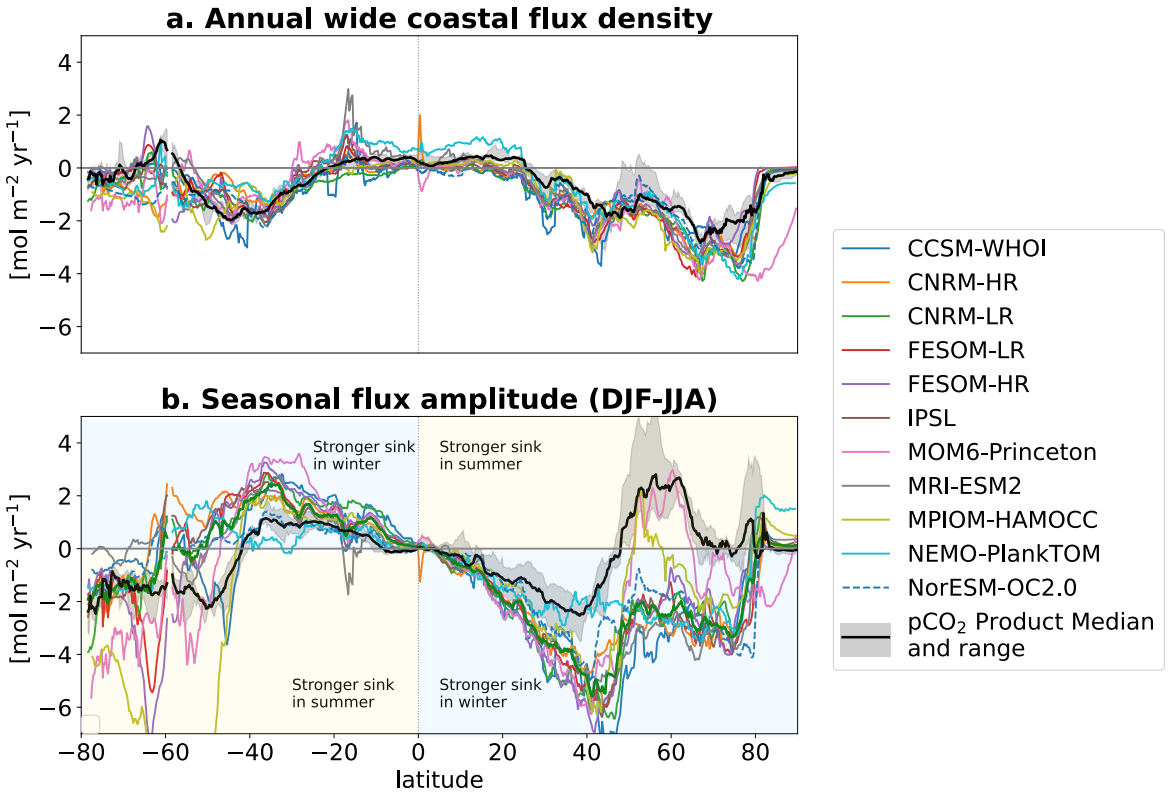

Figure S9. Latitudinal distribution of coastal ocean (wide shelf) a) annual mean CO_2 flux densities, b) CO_2 flux densities seasonal amplitude computed as December-February minus June-August, for the pCO_2 -product median and range (black line and grey shading) and each individual models (colored lines).

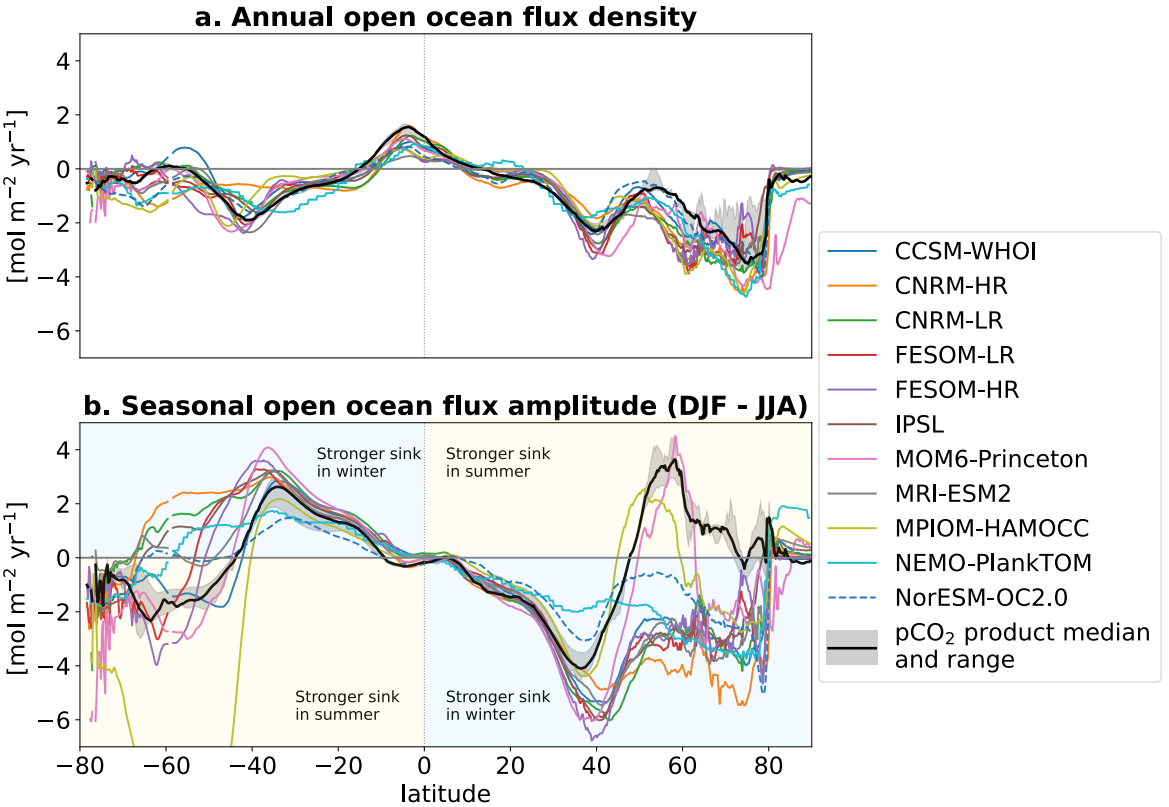

Figure S10. Latitudinal distribution of open ocean a) annual mean CO_2 flux densities, b) CO_2 flux densities seasonal amplitude computed as December-February minus June-August, for the pCO_2-product median (black line) and each individual models (colored lines). Note that the product median only includes the 3 (out of 4) products with open ocean values (CMEMS*, Carboscope-1 and Merged-SOM-FFN).

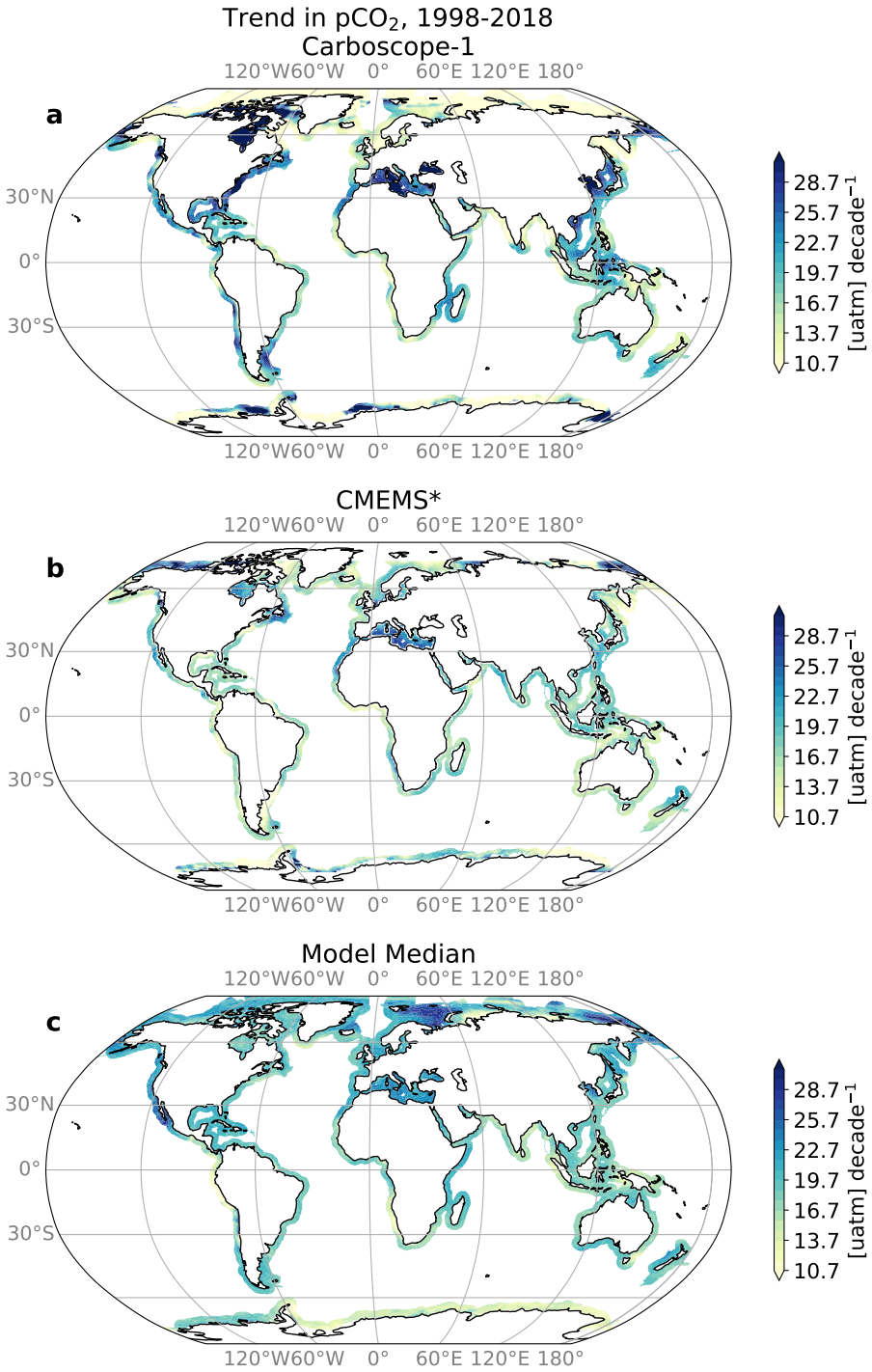

Figure S11. 1998-2018 trend in surface ocean pCO_2 in a) Carboscope-1 ; b) CMEMS* (area north of 75°N removed) c) multi-model median (global and regional models).

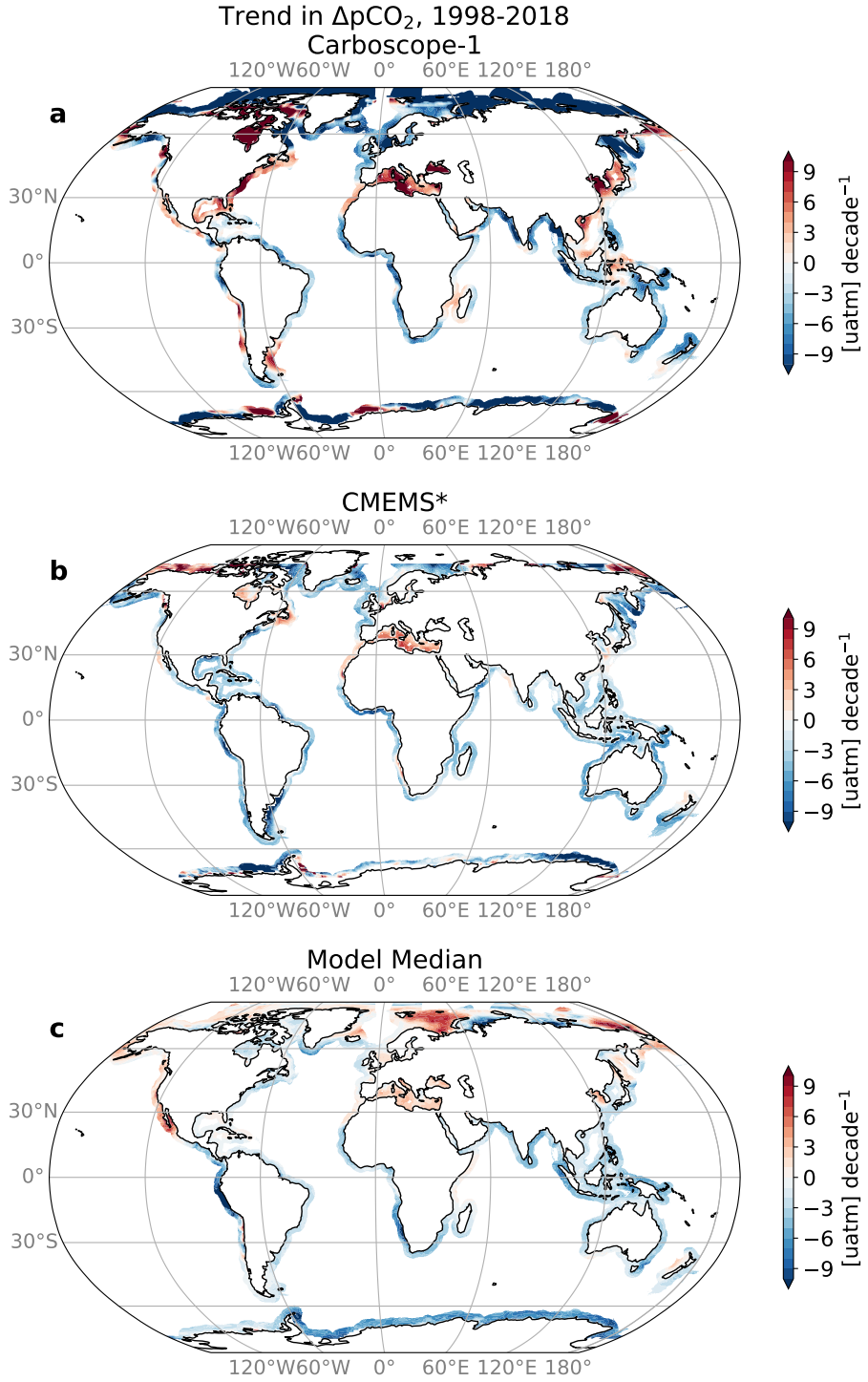

Figure S12. 1998-2018 trend in ΔpCO_2 (difference between coastal ocean surface ocean pCO_2 and atmospheric) for a) Carboscope-1; b) CMEMS* (area north of 75°N removed) c) multi-model median (global and regional models). Negative ΔpCO_2 trend values indicate that ocean pCO_2 increases at a lower rate than atmospheric and would therefore favor ocean uptake assuming constant wind and sea-ice coverage.

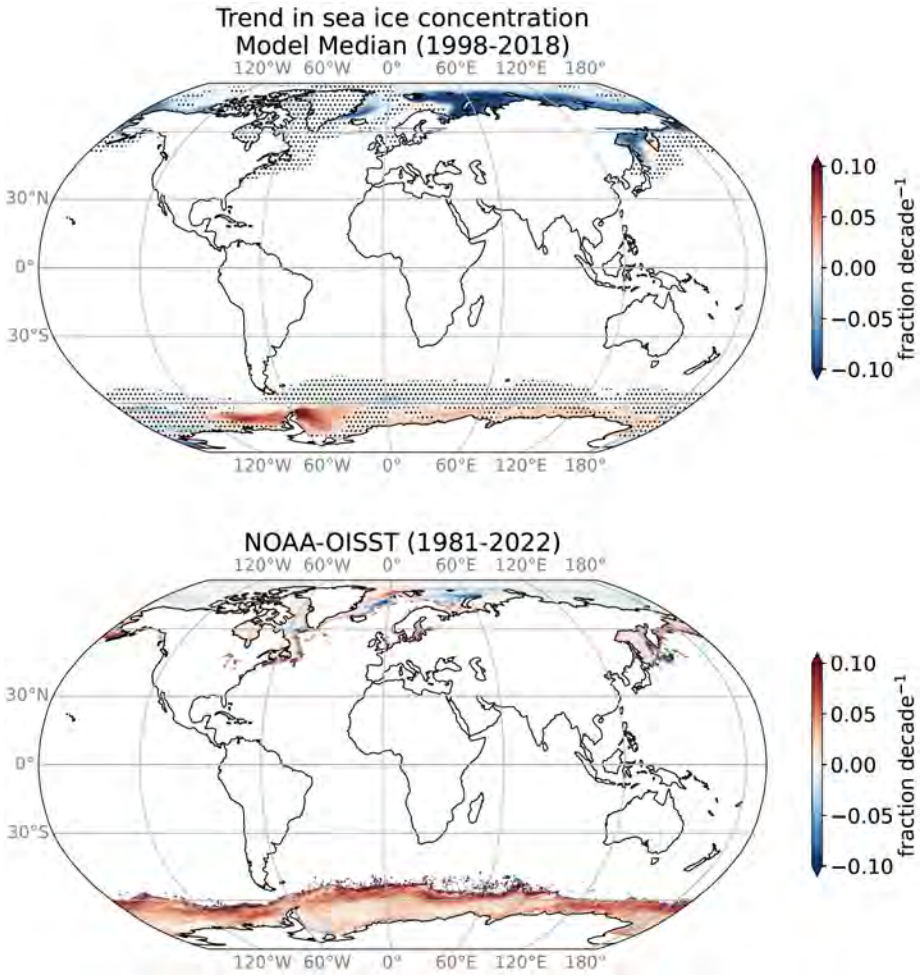

Figure S13. Linear trends in sea ice fraction from all 15 models median (top) and observation-based reference product NOAA-OISST (bottom). Stippling indicates where less than 6 out of the 11 global models agree on the sign of change.

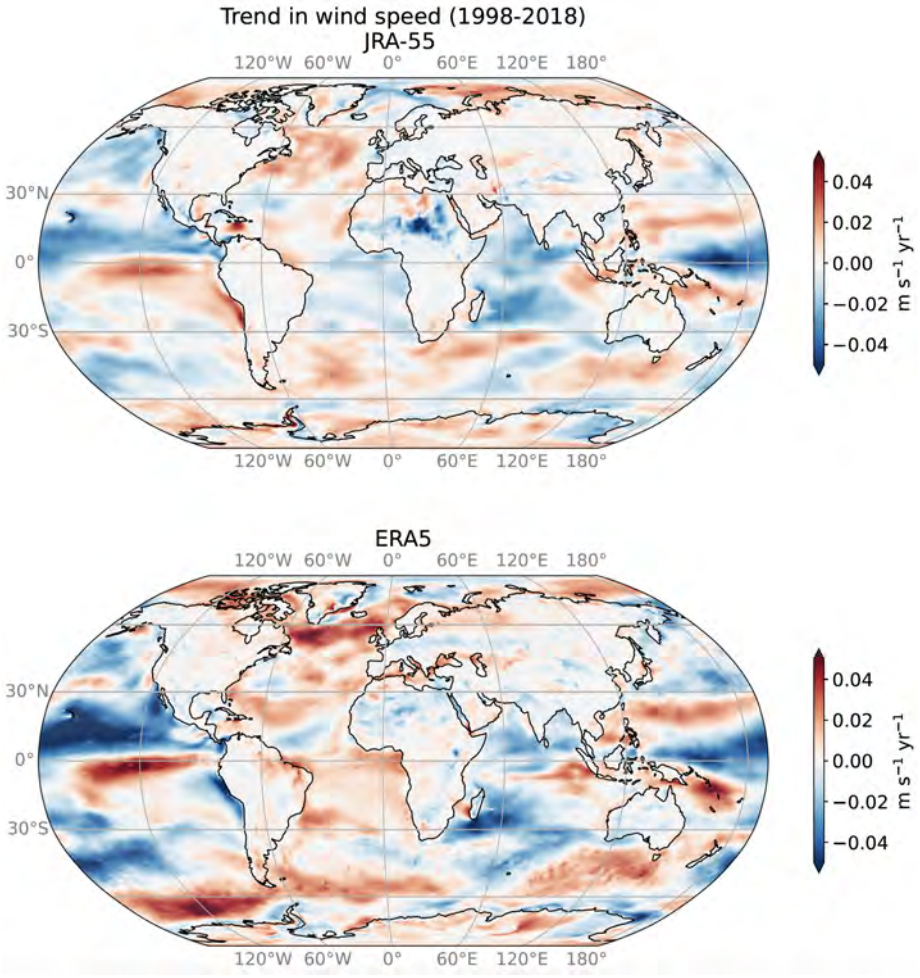

Figure S14. Linear trends in 10-meter wind speed from Japanese reanalysis JRA-55 (top) and ECMWF Reanalysis ERA-5 (bottom).

Table S2. Estimates of mean coastal ocean CO_2 flux densities, net CO_2 uptake and pCO_2 trends published since RECCAP-1 (Chen et al., 2013) and used in figures in the main text. Most prior estimates are given for coastal ocean areas similar to the area of the narrow coastal ocean used in this study (i.e. 28 million km^2).

Study	Mean coastal CO_2 flux density [mol m^{-2} yr^{-1}]	Net coastal CO_2 uptake [PgC yr^{-1}]	Coastal pCO_2 trends [uatm/decade]	Coastal area [million km^2]
Chen et al. (2013)	-1.09±2.9	-0.25±0.05	NA	30
Bauer et al. (2013)	NA	-0.25	NA	26
Laruelle et al. (2013)	-0.7	NA	NA	NA
Regnier et al. (2013)	NA	-0.2	NA	31
Laruelle et al. (2014)	-0.56 (global shelf) -0.7 (ice-free shelf)	-0.19±0.5 (1990-2011)	NA	28 22
Bourgeois et al. (2016)	NA	-0.1 (1993-2012)	NA	27
H. Wang et al. (2017)	NA	NA	+19.3±15.9 (from 10-30yr intervals in 1957-2014)	NA
Laruelle et al. (2018)	NA	-0.26 winter only	+13 [-6 to +32] winter only 1995-2006	30 (only 14 covered by obs. used)
Lacroix et al. (2021)	NA	-0.15 (1998-2015)	NA	24.5
Dai et al. (2022)	-0.68±0.14	-0.25±0.05 (1998-2021)	NA	30.32
Regnier et al. (2022)	NA	-0.32±0.08 (1990-2020)	NA	28

References

Adcroft, A., Anderson, W., Balaji, V., Blanton, C., Bushuk, M., Dufour, C. O., ... Zhang, R. (2019). The GFDL Global Ocean and Sea Ice Model OM4.0: Model Description and Simulation Features. *Journal of Advances in Modeling Earth Systems*, *11*(10), 3167–3211. Retrieved 2020-10-02, from https://agupubs.onlinelibrary.wiley.com/doi/abs/10.1029/2019MS001726 doi: 10.1029/2019MS001726

Araujo, M., Noriega, C., & Lefevre, N. (2014, May). Nutrients and carbon fluxes in the estuaries of major rivers flowing into the tropical Atlantic. *Frontiers in Marine Science*, *1*. Retrieved 2023-02-15, from http://journal.frontiersin.org/article/10.3389/fmars.2014.00010/abstract doi: 10.3389/fmars.2014.00010

Armstrong, R. A., Lee, C., Hedges, J. I., Honjo, S., & Wakeham, S. G. (2001, January). A new, mechanistic model for organic carbon fluxes in the ocean based on the quantitative association of POC with ballast minerals. *Deep Sea Research Part II: Topical Studies in Oceanography*, *49*(1-3), 219–236. Retrieved 2023-02-15, from https://linkinghub.elsevier.com/retrieve/pii/S0967064501001011 doi: 10.1016/S0967-0645(01)00101-1

Aumont, O., Ethé, C., Tagliabue, A., Bopp, L., & Gehlen, M. (2015, August). PISCES-v2: an ocean biogeochemical model for carbon and ecosystem studies. *Geoscientific Model Development*, *8*(8), 2465–2513. Retrieved 2023-02-15, from https://gmd.copernicus.org/articles/8/2465/2015/gmd-8-2465-2015.html (Publisher: Copernicus GmbH) doi: 10.5194/gmd-8-2465-2015

Bakker, D. C. E., Pfeil, B., Landa, C. S., Metzl, N., O'Brien, K. M., Olsen, A., ... Xu, S. (2016, September). A multi-decade record of high-quality fCO_2 data in version 3 of the Surface Ocean CO_2 Atlas (SOCAT). *Earth System Science Data*, *8*(2), 383–413. Retrieved from https://www.earth-syst-sci-data.net/8/383/2016/ doi: https://doi.org/10.5194/essd-8-383-2016

Barnier, B., Madec, G., Penduff, T., Molines, J., Treguier, A.-M., Le Sommer, J., ... de Cuevas, B. (2006, December). Impact of partial steps and momentum advection schemes in a global ocean circulation model at eddy-permitting resolution. *Ocean Dynamics*, *56*(5-6), 543–567. Retrieved 2023-02-15, from https://archimer.ifremer.fr/doc/00000/3514/ (Publisher: Springer) doi: 10.1007/s10236-006-0082-1

Bauer, J. E., Cai, W.-J., Raymond, P. A., Bianchi, T. S., Hopkinson, C. S., & Regnier, P. A. G. (2013, December). The changing carbon cycle of the coastal ocean. *Nature*, *504*(7478), 61–70. Retrieved 2016-01-12, from http://www.nature.com/nature/journal/v504/n7478/abs/nature12857.html doi: 10.1038/nature12857

Bernard, B., Madec, G., Penduff, T., Molines, J.-M., Treguier, A.-M., Le Sommer, J., ... De Cuevas, B. (2006, December). Impact of partial steps and momentum advection schemes in a global ocean circulation model at eddy-permitting resolution. *Ocean Dynamics*, *56*(5), 543–567. Retrieved 2023-02-15, from https://doi.org/10.1007/s10236-006-0082-1 doi: 10.1007/s10236-006-0082-1

Berthet, S., Jouanno, J., Séférian, R., Gehlen, M., & Llovel, W. (2022, August). How does the phytoplankton-light feedback affect marine N_2O inventory? *Earth Syst. Dynam. Discuss.*. Retrieved 2023-03-01, from https://esd.copernicus.org/preprints/

esd-2022-28/ doi: 10.5194/esd-2022-28

Berthet, S., Séférian, R., Bricaud, C., Chevallier, M., Voldoire, A., & Ethé, C. (2019, June). Evaluation of an Online Grid-Coarsening Algorithm in a Global Eddy-Admitting Ocean Biogeochemical Model. *Journal of Advances in Modeling Earth Systems*, *11*(6), 1759–1783. Retrieved 2023-03-01, from https://onlinelibrary.wiley.com/doi/abs/10.1029/2019MS001644 doi: 10.1029/2019MS001644

Bourgeois, T., Orr, J. C., Resplandy, L., Terhaar, J., Ethé, C., Gehlen, M., & Bopp, L. (2016, July). Coastal-ocean uptake of anthropogenic carbon. *Biogeosciences*, *13*(14), 4167–4185. Retrieved 2016-09-23, from http://www.biogeosciences.net/13/4167/2016/ doi: 10.5194/bg-13-4167-2016

Brennan, C. E., Bianucci, L., & Fennel, K. (2016, May). Sensitivity of Northwest North Atlantic Shelf Circulation to Surface and Boundary Forcing: A Regional Model Assessment. *Atmosphere-Ocean*, *54*(3), 230–247. Retrieved 2023-02-15, from https://www.tandfonline.com/doi/full/10.1080/07055900.2016.1147416 doi: 10.1080/07055900.2016.1147416

Buitenhuis, E. T., Le Quéré, C., Bednaršek, N., & Schiebel, R. (2019, March). Large Contribution of Pteropods to Shallow CaCO 3 Export. *Global Biogeochemical Cycles*, *33*(3), 458–468. Retrieved 2023-02-15, from https://onlinelibrary.wiley.com/doi/abs/10.1029/2018GB006110 doi: 10.1029/2018GB006110

Buitenhuis, E. T., Suntharalingam, P., & Le Quéré, C. (2018, April). Constraints on global oceanic emissions of N2O from observations and models. *Biogeosciences*, *15*(7), 2161–2175. Retrieved 2023-02-07, from https://bg.copernicus.org/articles/15/2161/2018/ (Publisher: Copernicus GmbH) doi: 10.5194/bg-15-2161-2018

Carroll, D., Menemenlis, D., Adkins, J. F., Bowman, K. W., Brix, H., Dutkiewicz, S., ... Zhang, H. (2020, October). The ECCO-Darwin Data-Assimilative Global Ocean Biogeochemistry Model: Estimates of Seasonal to Multidecadal Surface Ocean p CO 2 and Air-Sea CO 2 Flux. *Journal of Advances in Modeling Earth Systems*, *12*(10). Retrieved 2023-02-15, from https://onlinelibrary.wiley.com/doi/10.1029/2019MS001888 doi: 10.1029/2019MS001888

Chau, T. T. T., Gehlen, M., & Chevallier, F. (2022, February). A seamless ensemble-based reconstruction of surface ocean pCO2and air–sea CO2 fluxes over the global coastal and open oceans. *Biogeosciences*, *19*(4), 1087–1109. Retrieved 2023-02-15, from https://bg.copernicus.org/articles/19/1087/2022/ doi: 10.5194/bg-19-1087-2022

Chen, C.-T. A., Huang, T.-H., Chen, Y.-C., Bai, Y., He, X., & Kang, Y. (2013, October). Air–sea exchanges of CO2 in the world's coastal seas. *Biogeosciences*, *10*(10), 6509–6544. Retrieved 2021-09-03, from https://bg.copernicus.org/articles/10/6509/2013/ doi: 10.5194/bg-10-6509-2013

Dai, M., Su, J., Zhao, Y., Hofmann, E. E., Cao, Z., Cai, W.-J., ... Wang, Z. (2022). Carbon Fluxes in the Coastal Ocean: Synthesis, Boundary Processes, and Future Trends. *Annual Review of Earth and Planetary Sciences*, *50*(1), 593–626. Retrieved 2022-09-26, from https://doi.org/10.1146/annurev-earth-032320-090746 (_eprint: https://doi.org/10.1146/annurev-earth-032320-090746) doi: 10.1146/annurev-earth-032320-090746

Dee, D. P., Uppala, S. M., Simmons, A. J., Berrisford, P., Poli, P., Kobayashi, S., ... Vitart, F. (2011, April). The ERA-Interim reanalysis: configuration and performance of the data assimilation system. *Quarterly Journal of the Royal Meteorological Society*, *137*(656), 553–597. Retrieved 2023-02-15, from https://onlinelibrary.wiley.com/doi/10.1002/qj.828 doi: 10.1002/qj.828

de Verneil, A., Lachkar, Z., Smith, S., & Lévy, M. (2022, February). Evaluating the Arabian Sea as a regional source of atmospheric CO₂: seasonal variability and drivers. *Biogeosciences*, *19*(3), 907–929. Retrieved 2023-02-15, from https://bg.copernicus.org/articles/19/907/2022/ doi: 10.5194/bg-19-907-2022

Dickson, A. G., Sabine, C. L., Christian, J. R., Bargeron, C. P., & Organization, N. P. M. S. (Eds.). (2007). *Guide to best practices for ocean CO2 measurements* (No. no. 3). Sidney, BC: North Pacific Marine Science Organization.

Doney, S. C., Lima, I., Feely, R. A., Glover, D. M., Lindsay, K., Mahowald, N., ... Wanninkhof, R. (2009, April). Mechanisms governing interannual variability in upper-ocean inorganic carbon system and air–sea CO2 fluxes: Physical climate and atmospheric dust. *Deep Sea Research Part II: Topical Studies in Oceanography*, *56*(8-10), 640–655. Retrieved 2018-09-13, from http://linkinghub.elsevier.com/retrieve/pii/S096706450800427X doi: 10.1016/j.dsr2.2008.12.006

Dunne, J. P., Horowitz, L. W., Adcroft, A. J., Ginoux, P., Held, I. M., John, J. G., ... Zhao, M. (2020). The GFDL Earth System Model Version 4.1 (GFDL-ESM 4.1): Overall Coupled Model De-

scription and Simulation Characteristics. *Journal of Advances in Modeling Earth Systems*, *12*(11), e2019MS002015. Retrieved 2021-10-11, from https://onlinelibrary.wiley.com/doi/abs/10.1029/2019MS002015 doi: 10.1029/2019MS002015

Dunne, J. P., Sarmiento, J. L., & Gnanadesikan, A. (2007, December). A synthesis of global particle export from the surface ocean and cycling through the ocean interior and on the seafloor. *Global Biogeochemical Cycles*, *21*(4), GB4006. Retrieved 2016-02-08, from http://onlinelibrary.wiley.com/doi/10.1029/2006GB002907/abstract doi: 10.1029/2006GB002907

Fennel, K., & Wilkin, J. (2009, September). Quantifying biological carbon export for the northwest North Atlantic continental shelves. *Geophysical Research Letters*, *36*(18), L18605. Retrieved 2023-02-15, from http://doi.wiley.com/10.1029/2009GL039818 doi: 10.1029/2009GL039818

Fennel, K., Wilkin, J., Levin, J., Moisan, J., O'Reilly, J., & Haidvogel, D. (2006, September). Nitrogen cycling in the Middle Atlantic Bight: Results from a three-dimensional model and implications for the North Atlantic nitrogen budget: NITROGEN CYCLING IN THE MIDDLE ATLANTIC. *Global Biogeochemical Cycles*, *20*(3), n/a–n/a. Retrieved 2023-02-15, from http://doi.wiley.com/10.1029/2005GB002456 doi: 10.1029/2005GB002456

Franco, A. C., Gruber, N., Frölicher, T. L., & Kropuenske Artman, L. (2018, March). Contrasting Impact of Future CO_2 Emission Scenarios on the Extent of $CaCO_3$ Mineral Undersaturation in the Humboldt Current System. *Journal of Geophysical Research: Oceans*, *123*(3), 2018–2036. Retrieved 2023-02-15, from http://doi.wiley.com/10.1002/2018JC013857 doi: 10.1002/2018JC013857

Friedlingstein, P., Jones, M. W., O'Sullivan, M., Andrew, R. M., Bakker, D. C. E., Hauck, J., ... Zeng, J. (2022, April). Global Carbon Budget 2021. *Earth System Science Data*, *14*(4), 1917–2005. Retrieved 2023-05-19, from https://essd.copernicus.org/articles/14/1917/2022/ (Publisher: Copernicus GmbH) doi: 10.5194/essd-14-1917-2022

Friedlingstein, P., O'Sullivan, M., Jones, M. W., Andrew, R. M., Hauck, J., Olsen, A., ... Zaehle, S. (2020, December). Global Carbon Budget 2020. *Earth System Science Data*, *12*(4), 3269–3340. Retrieved 2021-08-31, from https://essd.copernicus.org/articles/12/3269/2020/ doi: 10.5194/essd-12-3269-2020

Frischknecht, M. (2018). *New Perspectives on the Three-Dimensional Cycling of Carbon and Nutrients in the California Current System and its Response to ENSO* (Doctoral dissertation, ETH Zurich). (Artwork Size: 254 p. Medium: application/pdf Pages: 254 p.) doi: 10.3929/ETHZ-B-000283522

Ganesan, A. L., Manizza, M., Morgan, E. J., Harth, C. M., Kozlova, E., Lueker, T., ... Rigby, M. (2020, July). Marine Nitrous Oxide Emissions From Three Eastern Boundary Upwelling Systems Inferred From Atmospheric Observations. *Geophysical Research Letters*, *47*(14). Retrieved 2023-02-15, from https://onlinelibrary.wiley.com/doi/10.1029/2020GL087822 doi: 10.1029/2020GL087822

Garcia, H. E., Locarnini, R. A., Boyer, T. P., Baranova, O. K., Zweng, M. M., Reagan, J. R., & Johnson, D. R. (2014). *World Ocean Atlas 2013, Volume 3: Dissolved Oxygen, Apparent Oxygen Utilization, and Oxygen Saturation.* (Tech. Rep.). S. Levitus, Ed., A. Mishonov Technical Ed.; NOAA Atlas NESDIS 75, 27 pp.

Good, S., Fiedler, E., Mao, C., Martin, M. J., Maycock, A., Reid, R., ... Worsfold, M. (2020, February). The Current Configuration of the OSTIA System for Operational Production of Foundation Sea Surface Temperature and Ice Concentration Analyses. *Remote Sensing*, *12*(4), 720. Retrieved 2023-02-14, from https://www.mdpi.com/2072-4292/12/4/720 doi: 10.3390/rs12040720

Good, S. A., Martin, M. J., & Rayner, N. A. (2013, December). EN4: Quality controlled ocean temperature and salinity profiles and monthly objective analyses with uncertainty estimates: THE EN4 DATA SET. *Journal of Geophysical Research: Oceans*, *118*(12), 6704–6716. Retrieved 2023-02-15, from http://doi.wiley.com/10.1002/2013JC009067 doi: 10.1002/2013JC009067

Gruber, N., Clement, D., Carter, B. R., Feely, R. A., Heuven, S. v., Hoppema, M., ... Wanninkhof, R. (2019, March). The oceanic sink for anthropogenic CO2 from 1994 to 2007. *Science*, *363*(6432), 1193–1199. Retrieved 2019-03-19, from http://science.sciencemag.org.ezproxy.princeton.edu/content/363/6432/1193 doi: 10.1126/science.aau5153

Gruber, N., Frenzel, H., Doney, S. C., Marchesiello, P., McWilliams, J. C., Moisan, J. R., ... Stolzenbach, K. D. (2006, September). Eddy-resolving simulation of plankton ecosystem dynamics in the California Current System. *Deep Sea Research Part I: Oceanographic Research Papers*, *53*(9), 1483–1516. Retrieved 2023-02-15, from https://www.sciencedirect.com/

science/article/pii/S0967063706001713 doi: 10.1016/j.dsr.2006.06.005

Gruber, N., Hauri, C., Lachkar, Z., Loher, D., Frölicher, T. L., & Plattner, G.-K. (2012, July). Rapid Progression of Ocean Acidification in the California Current System. *Science*, *337*(6091), 220–223. Retrieved 2023-02-15, from https://www.science.org/doi/10.1126/science.1216773 doi: 10.1126/science.1216773

Haidvogel, D., Arango, H., Budgell, W., Cornuelle, B., Curchitser, E., Di Lorenzo, E., ... Wilkin, J. (2008, March). Ocean forecasting in terrain-following coordinates: Formulation and skill assessment of the Regional Ocean Modeling System. *Journal of Computational Physics*, *227*(7), 3595–3624. Retrieved 2023-02-15, from https://linkinghub.elsevier.com/retrieve/pii/S0021999107002549 doi: 10.1016/j.jcp.2007.06.016

Hartmann, J., Jansen, N., Dürr, H. H., Kempe, S., & Köhler, P. (2009, December). Global CO2-consumption by chemical weathering: What is the contribution of highly active weathering regions? *Global and Planetary Change*, *69*(4), 185–194. Retrieved 2020-01-30, from https://linkinghub.elsevier.com/retrieve/pii/S0921818109001349 doi: 10.1016/j.gloplacha.2009.07.007

Hauck, J., Völker, C., Wang, T., Hoppema, M., Losch, M., & Wolf-Gladrow, D. A. (2013, December). Seasonally different carbon flux changes in the Southern Ocean in response to the southern annular mode. *Global Biogeochemical Cycles*, *27*(4), 1236–1245. Retrieved 2023-02-15, from https://onlinelibrary.wiley.com/doi/10.1002/2013GB004600 doi: 10.1002/2013GB004600

Hauck, J., Zeising, M., Le Quéré, C., Gruber, N., Bakker, D. C. E., Bopp, L., ... Séférian, R. (2020). Consistency and Challenges in the Ocean Carbon Sink Estimate for the Global Carbon Budget. *Frontiers in Marine Science*, *7*. Retrieved 2020-12-18, from https://www.frontiersin.org/articles/10.3389/fmars.2020.571720/full (Publisher: Frontiers) doi: 10.3389/fmars.2020.571720

Hersbach, H., Bell, B., Berrisford, P., Hirahara, S., Horányi, A., Muñoz-Sabater, J., ... Thépaut, J.-N. (2020). The ERA5 global reanalysis. *Quarterly Journal of the Royal Meteorological Society*, *146*(730), 1999–2049. Retrieved 2023-02-14, from https://onlinelibrary.wiley.com/doi/abs/10.1002/qj.3803 doi: 10.1002/qj.3803

Ho, D. T., Law, C. S., Smith, M. J., Schlosser, P., Harvey, M., & Hill, P. (2006). Measurements of air-sea gas exchange at high wind speeds in the Southern Ocean: Implications for global parameterizations. *Geophysical Research Letters*, *33*(16). Retrieved 2019-06-25, from https://agupubs.onlinelibrary.wiley.com/doi/abs/10.1029/2006GL026817 doi: 10.1029/2006GL026817

Ho, D. T., Wanninkhof, R., Schlosser, P., Ullman, D. S., Hebert, D., & Sullivan, K. F. (2011, July). Toward a universal relationship between wind speed and gas exchange: Gas transfer velocities measured with ^{3}He/SF$_{6}$ during the Southern Ocean Gas Exchange Experiment. *Journal of Geophysical Research*, *116*, C00F04. Retrieved 2023-02-15, from http://doi.wiley.com/10.1029/2010JC006854 doi: 10.1029/2010JC006854

Hornafius, J. S., Quigley, D., & Luyendyk, B. P. (1999, September). The world's most spectacular marine hydrocarbon seeps (Coal Oil Point, Santa Barbara Channel, California): Quantification of emissions. *Journal of Geophysical Research: Oceans*, *104*(C9), 20703–20711. Retrieved 2023-02-23, from http://doi.wiley.com/10.1029/1999JC900148 doi: 10.1029/1999JC900148

Hovland, M., Judd, A., & Burke, R. (1993, January). The global flux of methane from shallow submarine sediments. *Chemosphere*, *26*(1-4), 559–578. Retrieved 2023-02-23, from https://linkinghub.elsevier.com/retrieve/pii/0045653593904428 doi: 10.1016/0045-6535(93)90442-8

Ilyina, T., Six, K. D., Segschneider, J., Maier-Reimer, E., Li, H., & Núñez-Riboni, I. (2013, June). Global ocean biogeochemistry model HAMOCC: Model architecture and performance as component of the MPI-Earth system model in different CMIP5 experimental realizations. *Journal of Advances in Modeling Earth Systems*, *5*(2), 287–315. Retrieved 2023-02-15, from https://onlinelibrary.wiley.com/doi/10.1029/2012MS000178 doi: 10.1029/2012MS000178

Joos, F., & Spahni, R. (2008, February). Rates of change in natural and anthropogenic radiative forcing over the past 20,000 years. *Proceedings of the National Academy of Sciences*, *105*(5), 1425–1430. Retrieved 2019-06-18, from https://www.pnas.org/content/105/5/1425 doi: 10.1073/pnas.0707386105

Jungclaus, J. H., Fischer, N., Haak, H., Lohmann, K., Marotzke, J., Matei, D., ... Storch, J. S. (2013, June). Characteristics of the ocean simulations in the Max Planck Institute Ocean Model (MPIOM) the ocean component of the MPI-Earth system model. *Journal of Advances in Modeling Earth Systems*, *5*(2), 422–446. Retrieved 2023-02-20,

from https://onlinelibrary.wiley.com/doi/10.1002/jame.20023 doi: 10.1002/jame.20023

Kanamitsu, M., Ebisuzaki, W., Woollen, J., Yang, S.-K., Hnilo, J. J., Fiorino, M., & Potter, G. L. (2002, November). NCEP–DOE AMIP-II Reanalysis (R-2). *Bulletin of the American Meteorological Society*, *83*(11), 1631–1644. Retrieved 2023-02-15, from https://journals.ametsoc.org/view/journals/bams/83/11/bams-83-11-1631.xml (Publisher: American Meteorological Society Section: Bulletin of the American Meteorological Society) doi: 10.1175/BAMS-83-11-1631

Keeling, C. D., Piper, S. C., Bacastow, R. B., Wahlen, M., Whorf, T. P., Heimann, M., & Meijer, H. A. (2005). Atmospheric CO_2 and $13CO_2$ Exchange with the Terrestrial Biosphere and Oceans from 1978 to 2000: Observations and Carbon Cycle Implications. In I. T. Baldwin et al. (Eds.), *A History of Atmospheric CO2 and Its Effects on Plants, Animals, and Ecosystems* (pp. 83–113). Springer New York. Retrieved 2016-09-16, from http://link.springer.com/chapter/10.1007/0-387-27048-5_5 doi: 10.1007/0-387-27048-5_5

Key, R. M., Kozyr, A., Sabine, C. L., Lee, K., Wanninkhof, R., Bullister, J. L., ... Peng, T.-H. (2004, December). A global ocean carbon climatology: Results from Global Data Analysis Project (GLODAP): GLOBAL OCEAN CARBON CLIMATOLOGY. *Global Biogeochemical Cycles*, *18*(4), n/a–n/a. Retrieved 2023-02-15, from http://doi.wiley.com/10.1029/2004GB002247 doi: 10.1029/2004GB002247

Khatiwala, S., Tanhua, T., Mikaloff Fletcher, S., Gerber, M., Doney, S. C., Graven, H. D., ... Sabine, C. L. (2013, April). Global ocean storage of anthropogenic carbon. *Biogeosciences*, *10*(4), 2169–2191. Retrieved 2016-01-19, from http://www.biogeosciences.net/10/2169/2013/ doi: 10.5194/bg-10-2169-2013

Kock, A., & Bange, H. (2015, February). Counting the Ocean's Greenhouse Gas Emissions. *Eos*, *96*. Retrieved 2023-02-14, from https://eos.org/project-updates/counting-oceans-greenhouse-gas-emissions doi: 10.1029/2015EO023665

Krishna, M., Prasad, M., Rao, D., Viswanadham, R., Sarma, V., & Reddy, N. (2016, January). Export of dissolved inorganic nutrients to the northern Indian Ocean from the Indian monsoonal rivers during discharge period. *Geochimica et Cosmochimica Acta*, *172*, 430–443. Retrieved 2023-02-23, from https://linkinghub.elsevier.com/retrieve/pii/S0016703715005955 doi: 10.1016/j.gca.2015.10.013

Lachkar, Z., & Gruber, N. (2013, January). Response of biological production and air–sea CO2 fluxes to upwelling intensification in the California and Canary Current Systems. *Journal of Marine Systems*, *109-110*, 149–160. Retrieved 2023-02-15, from https://www.sciencedirect.com/science/article/pii/S092479631200108X doi: 10.1016/j.jmarsys.2012.04.003

Lachkar, Z., Mehari, M., Al Azhar, M., Lévy, M., & Smith, S. (2021, October). Fast local warming is the main driver of recent deoxygenation in the northern Arabian Sea. *Biogeosciences*, *18*(20), 5831–5849. Retrieved 2023-02-15, from https://bg.copernicus.org/articles/18/5831/2021/ doi: 10.5194/bg-18-5831-2021

Lachkar, Z., Smith, S., Lévy, M., & Pauluis, O. (2016, September). Eddies reduce denitrification and compress habitats in the Arabian Sea. *Geophysical Research Letters*, *43*(17), 9148–9156. Retrieved 2018-01-16, from http://onlinelibrary.wiley.com/doi/10.1002/2016GL069876/full doi: 10.1002/2016GL069876

Lacroix, F., Ilyina, T., Laruelle, G. G., & Regnier, P. (2021). Reconstructing the Preindustrial Coastal Carbon Cycle Through a Global Ocean Circulation Model: Was the Global Continental Shelf Already Both Autotrophic and a CO2 Sink? *Global Biogeochemical Cycles*, *35*(2), e2020GB006603. Retrieved 2021-09-03, from https://agupubs.onlinelibrary.wiley.com/doi/abs/10.1029/2020GB006603 doi: 10.1029/2020GB006603

Landschützer, P., Gruber, N., Bakker, D. C. E., & Schuster, U. (2014, September). Recent variability of the global ocean carbon sink. *Global Biogeochemical Cycles*, *28*(9), 927–949. Retrieved 2015-08-11, from http://onlinelibrary.wiley.com/doi/10.1002/2014GB004853/abstract doi: 10.1002/2014GB004853

Landschützer, P., Gruber, N., Bakker, D. C. E., Schuster, U., Nakaoka, S., Payne, M. R., ... Zeng, J. (2013, November). A neural network-based estimate of the seasonal to inter-annual variability of the Atlantic Ocean carbon sink. *Biogeosciences*, *10*(11), 7793–7815. Retrieved 2023-02-15, from https://bg.copernicus.org/articles/10/7793/2013/ doi: 10.5194/bg-10-7793-2013

Landschützer, P., Laruelle, G. G., Roobaert, A., & Regnier, P. (2020, October). A uniform pCO2 climatology combining open and coastal oceans. *Earth System Science Data*, *12*(4), 2537–2553. Retrieved 2023-02-14, from https://essd.copernicus.org/

articles/12/2537/2020/ doi: 10.5194/essd-12-2537-2020

Large, W. G., McWilliams, J. C., & Doney, S. C. (1994). Oceanic vertical mixing: A review and a model with a nonlocal boundary layer parameterization. *Reviews of Geophysics*, *32*(4), 363–403. Retrieved 2023-02-15, from https://onlinelibrary.wiley.com/doi/abs/10.1029/94RG01872 doi: 10.1029/94RG01872

Large, W. G., & Yeager, S. G. (2009, August). The global climatology of an interannually varying air–sea flux data set. *Climate Dynamics*, *33*(2-3), 341–364. Retrieved 2015-04-02, from http://link.springer.com/10.1007/s00382-008-0441-3 doi: 10.1007/s00382-008-0441-3

Laruelle, G. G., Cai, W.-J., Hu, X., Gruber, N., Mackenzie, F. T., & Regnier, P. (2018, January). Continental shelves as a variable but increasing global sink for atmospheric carbon dioxide. *Nature Communications*, *9*, 454. Retrieved 2021-09-03, from https://www.ncbi.nlm.nih.gov/pmc/articles/PMC5792465/ doi: 10.1038/s41467-017-02738-z

Laruelle, G. G., Dürr, H. H., Lauerwald, R., Hartmann, J., Slomp, C. P., Goossens, N., & Regnier, P. A. G. (2013, May). Global multi-scale segmentation of continental and coastal waters from the watersheds to the continental margins. *Hydrology and Earth System Sciences*, *17*(5), 2029–2051. Retrieved 2020-03-27, from https://www.hydrol-earth-syst-sci.net/17/2029/2013/ doi: 10.5194/hess-17-2029-2013

Laruelle, G. G., Landschützer, P., Gruber, N., Tison, J.-L., Delille, B., & Regnier, P. (2017, October). Global high-resolution monthly pCO2 climatology for the coastal ocean derived from neural network interpolation. *Biogeosciences*, *14*(19), 4545–4561. Retrieved 2019-08-29, from https://www.biogeosciences.net/14/4545/2017/ doi: 10.5194/bg-14-4545-2017

Laruelle, G. G., Lauerwald, R., Pfeil, B., & Regnier, P. (2014). Regionalized global budget of the CO2 exchange at the air-water interface in continental shelf seas. *Global Biogeochemical Cycles*, *28*(11), 1199–1214. Retrieved 2021-09-03, from https://agupubs.onlinelibrary.wiley.com/doi/abs/10.1002/2014GB004832 doi: 10.1002/2014GB004832

Laurent, A., Fennel, K., Cai, W., Huang, W., Barbero, L., & Wanninkhof, R. (2017, January). Eutrophication-induced acidification of coastal waters in the northern Gulf of Mexico: Insights into origin and processes from a coupled physical-biogeochemical model. *Geophysical Research Letters*, *44*(2), 946–956. Retrieved 2023-02-15, from https://onlinelibrary.wiley.com/doi/abs/10.1002/2016GL071881 doi: 10.1002/2016GL071881

Laurent, A., Fennel, K., & Kuhn, A. (2021, March). An observation-based evaluation and ranking of historical Earth system model simulations in the northwest North Atlantic Ocean. *Biogeosciences*, *18*(5), 1803–1822. Retrieved 2023-02-15, from https://bg.copernicus.org/articles/18/1803/2021/ doi: 10.5194/bg-18-1803-2021

Lauvset, S. K., Key, R. M., Olsen, A., Heuven, S. v., Velo, A., Lin, X., ... Watelet, S. (2016, August). A new global interior ocean mapped climatology: the 1° × 1° GLODAP version 2. *Earth System Science Data*, *8*(2), 325–340. Retrieved 2016-11-07, from http://www.earth-syst-sci-data.net/8/325/2016/ doi: 10.5194/essd-8-325-2016

Liang, J.-H., Deutsch, C., McWilliams, J. C., Baschek, B., Sullivan, P. P., & Chiba, D. (2013). Parameterizing bubble-mediated air-sea gas exchange and its effect on ocean ventilation. *Global Biogeochemical Cycles*, *27*(3), 894–905. Retrieved 2023-02-14, from https://onlinelibrary.wiley.com/doi/abs/10.1002/gbc.20080 doi: 10.1002/gbc.20080

Liao, E., Resplandy, L., Liu, J., & Bowman, K. W. (2020). Amplification of the Ocean Carbon Sink During El Niños: Role of Poleward Ekman Transport and Influence on Atmospheric CO2. *Global Biogeochemical Cycles*, *34*(9), e2020GB006574. Retrieved 2020-10-15, from http://agupubs.onlinelibrary.wiley.com/doi/abs/10.1029/2020GB006574 doi: 10.1029/2020GB006574

Liss, P. S., & Merlivat, L. (1986). Air-Sea Gas Exchange Rates: Introduction and Synthesis. In P. Buat-Ménard (Ed.), *The Role of Air-Sea Exchange in Geochemical Cycling* (pp. 113–127). Dordrecht: Springer Netherlands. Retrieved 2023-02-23, from https://doi.org/10.1007/978-94-009-4738-2_5 doi: 10.1007/978-94-009-4738-2_5

Locarnini, R. A., Mishonov, A. V., Antonov, J. I., Boyer, T. P., Garcia, H. E., Baranova, O. K., ... Seidov, D. (2014). *World Ocean Atlas 2013, Volume 1: Temperature.* (Tech. Rep.). S. Levitus, Ed., A. Mishonov Technical Ed.; NOAA Atlas NESDIS 73, 40 pp.

Louchard, D., Gruber, N., & Münnich, M. (2021). The Impact of the Amazon on the Biological Pump and the Air-Sea CO2 Balance of the Western Tropical Atlantic. *Global Biogeochemical Cycles*, *35*(6), e2020GB006818. Retrieved 2021-09-22, from https://onlinelibrary.wiley.com/

doi/abs/10.1029/2020GB006818 doi: 10.1029/2020GB006818

Ludwig, W., Amiotte Suchet, P., & Probst, J.-L. (1996). River discharges of carbon to the world's oceans: determining local inputs of alkalinity and of dissolved and particulate organic carbon. *Sciences de la terre et des planètes (Comptes rendus de l'Académie des sciences)*, *t. 323*, 1007–1014. Retrieved 2023-02-15, from https://oatao.univ-toulouse.fr/3498/ (Publisher: Gauthier-Villars)

Madec, G., Bourdallé-Badie, R., Bouttier, P.-A., Bricaud, C., Bruciaferri, D., Calvert, D., ... Vancoppenolle, M. (2017). NEMO ocean engine. Retrieved 2023-02-15, from https://zenodo.org/record/1472492 doi: 10.5281/ZENODO.1472492

Mahowald, N. M., Engelstaedter, S., Luo, C., Sealy, A., Artaxo, P., Benitez-Nelson, C., ... Siefert, R. L. (2009). Atmospheric Iron Deposition: Global Distribution, Variability, and Human Perturbations. *Annual Review of Marine Science*, *1*(1), 245–278. Retrieved 2023-02-21, from https://doi.org/10.1146/annurev.marine.010908.163727 doi: 10.1146/annurev.marine.010908.163727

Manizza, M., Keeling, R. F., & Nevison, C. D. (2012, January). On the processes controlling the seasonal cycles of the air–sea fluxes of O_2 and N_2O: A modelling study. *Tellus B: Chemical and Physical Meteorology*, *64*(1), 18429. Retrieved 2023-02-15, from https://b.tellusjournals.se/article/10.3402/tellusb.v64i0.18429/ doi: 10.3402/tellusb.v64i0.18429

Manizza, M., Menemenlis, D., Zhang, H., & Miller, C. E. (2019). Modeling the Recent Changes in the Arctic Ocean CO_2 Sink (2006–2013). *Global Biogeochemical Cycles*, *33*(3), 420–438. Retrieved 2023-02-15, from https://onlinelibrary.wiley.com/doi/abs/10.1029/2018GB006070 doi: 10.1029/2018GB006070

Martinez-Rey, J., Bopp, L., Gehlen, M., Tagliabue, A., & Gruber, N. (2015, July). Projections of oceanic N2O emissions in the 21st century using the IPSL Earth system model. *Biogeosciences*, *12*(13), 4133–4148. Retrieved 2016-06-07, from http://www.biogeosciences.net/12/4133/2015/ doi: 10.5194/bg-12-4133-2015

Mayorga, E., Seitzinger, S. P., Harrison, J. A., Dumont, E., Beusen, A. H., Bouwman, A., ... Van Drecht, G. (2010, July). Global Nutrient Export from WaterSheds 2 (NEWS 2): Model development and implementation. *Environmental Modelling & Software*, *25*(7), 837–853. Retrieved 2023-02-23, from https://linkinghub.elsevier.com/retrieve/pii/S1364815210000186 doi: 10.1016/j.envsoft.2010.01.007

McGinnis, D. F., Greinert, J., Artemov, Y., Beaubien, S. E., & Wüest, A. (2006). Fate of rising methane bubbles in stratified waters: How much methane reaches the atmosphere? *Journal of Geophysical Research*, *111*(C9), C09007. Retrieved 2023-02-23, from http://doi.wiley.com/10.1029/2005JC003183 doi: 10.1029/2005JC003183

Middelburg, J. J., Soetaert, K., Herman, P. M. J., & Heip, C. H. R. (1996, December). Denitrification in marine sediments: A model study. *Global Biogeochemical Cycles*, *10*(4), 661–673. Retrieved 2023-02-15, from http://doi.wiley.com/10.1029/96GB02562 doi: 10.1029/96GB02562

Moore, J. K., Lindsay, K., Doney, S. C., Long, M. C., & Misumi, K. (2013, August). Marine Ecosystem Dynamics and Biogeochemical Cycling in the Community Earth System Model [CESM1(BGC)]: Comparison of the 1990s with the 2090s under the RCP4.5 and RCP8.5 Scenarios. *Journal of Climate*, *26*(23), 9291–9312. Retrieved 2016-06-16, from http://journals.ametsoc.org/doi/abs/10.1175/JCLI-D-12-00566.1 doi: 10.1175/JCLI-D-12-00566.1

Naegler, T. (2009, January). Reconciliation of excess 14C-constrained global CO2 piston velocity estimates. *Tellus B: Chemical and Physical Meteorology*, *61*(2), 372–384. Retrieved 2023-02-15, from https://doi.org/10.1111/j.1600-0889.2008.00408.x (Publisher: Taylor & Francis _eprint: https://doi.org/10.1111/j.1600-0889.2008.00408.x) doi: 10.1111/j.1600-0889.2008.00408.x

Nakano, H., Tsujino, H., Hirabara, M., Yasuda, T., Motoi, T., Ishii, M., & Yamanaka, G. (2011, December). Uptake mechanism of anthropogenic CO2 in the Kuroshio Extension region in an ocean general circulation model. *Journal of Oceanography*, *67*(6), 765–783. Retrieved 2019-09-25, from https://doi.org/10.1007/s10872-011-0075-7 doi: 10.1007/s10872-011-0075-7

Nevison, C., Butler, J. H., & Elkins, J. W. (2003, December). Global distribution of N_2O and the N_2O-AOU yield in the subsurface ocean. *Global Biogeochemical Cycles*, *17*(4), n/a–n/a. Retrieved 2023-02-15, from http://doi.wiley.com/10.1029/2003GB002068 doi: 10.1029/2003GB002068

Nightingale, P. D., Malin, G., Law, C. S., Watson, A. J., Liss, P. S., Liddicoat, M. I., ... Upstill-Goddard, R. C. (2000, March). In situ evaluation of air-sea gas exchange parameterizations using novel conservative and volatile

tracers. *Global Biogeochemical Cycles*, *14*(1), 373–387. Retrieved 2023-02-15, from http://doi.wiley.com/10.1029/1999GB900091 doi: 10.1029/1999GB900091

Olsen, A., Key, R. M., van Heuven, S., Lauvset, S. K., Velo, A., Lin, X., ... Suzuki, T. (2016, August). The Global Ocean Data Analysis Project version 2 (GLODAPv2) – an internally consistent data product for the world ocean. *Earth System Science Data*, *8*(2), 297–323. Retrieved 2023-02-15, from https://essd.copernicus.org/articles/8/297/2016/ (Publisher: Copernicus GmbH) doi: 10.5194/essd-8-297-2016

Olsen, A., Lange, N., Key, R. M., Tanhua, T., Álvarez, M., Becker, S., ... Wanninkhof, R. (2019, September). GLODAPv2.2019 – an update of GLODAPv2. *Earth System Science Data*, *11*(3), 1437–1461. Retrieved 2023-02-16, from https://essd.copernicus.org/articles/11/1437/2019/ (Publisher: Copernicus GmbH) doi: 10.5194/essd-11-1437-2019

Orr, J. C., Epitalon, J.-M., & Gattuso, J.-P. (2015, March). Comparison of ten packages that compute ocean carbonate chemistry. *Biogeosciences*, *12*(5), 1483–1510. Retrieved 2023-02-15, from https://bg.copernicus.org/articles/12/1483/2015/ (Publisher: Copernicus GmbH) doi: 10.5194/bg-12-1483-2015

Orr, J. C., Fabry, V. J., Aumont, O., Bopp, L., Doney, S. C., Feely, R. A., ... Yool, A. (2005, September). Anthropogenic ocean acidification over the twenty-first century and its impact on calcifying organisms. *Nature*, *437*(7059), 681–686. Retrieved 2023-02-15, from https://www.nature.com/articles/nature04095 (Number: 7059 Publisher: Nature Publishing Group) doi: 10.1038/nature04095

Orr, J. C., Najjar, R. G., Aumont, O., Bopp, L., Bullister, J. L., Danabasoglu, G., ... Yool, A. (2017, June). Biogeochemical protocols and diagnostics for the CMIP6 Ocean Model Intercomparison Project (OMIP). *Geoscientific Model Development*, *10*(6), 2169–2199. Retrieved 2020-02-20, from https://www.geosci-model-dev.net/10/2169/2017/ doi: https://doi.org/10.5194/gmd-10-2169-2017

Paulsen, H., Ilyina, T., Six, K. D., & Stemmler, I. (2017, March). Incorporating a prognostic representation of marine nitrogen fixers into the global ocean biogeochemical model HAMOCC: PROGNOSTIC NITROGEN FIXERS IN HAMOCC. *Journal of Advances in Modeling Earth Systems*, *9*(1), 438–464. Retrieved 2023-02-20, from http://doi.wiley.com/10.1002/2016MS000737 doi: 10.1002/2016MS000737

Ramesh, R., Purvaja, G. R., & Subramanian, V. (1995). Carbon and Phosphorus Transport by the Major Indian Rivers. *Journal of Biogeography*, *22*(2/3), 409–415. Retrieved 2023-02-23, from https://www.jstor.org/stable/2845937 (Publisher: Wiley) doi: 10.2307/2845937

Regnier, P., Friedlingstein, P., Ciais, P., Mackenzie, F. T., Gruber, N., Janssens, I. A., ... Thullner, M. (2013, June). Anthropogenic perturbation of the carbon fluxes from land to ocean. *Nature Geoscience*, *6*(8), 597–607. Retrieved 2015-06-25, from http://www.nature.com/doifinder/10.1038/ngeo1830 doi: 10.1038/ngeo1830

Regnier, P., Resplandy, L., Najjar, R. G., & Ciais, P. (2022, March). The land-to-ocean loops of the global carbon cycle. *Nature*, *603*(7901), 401–410. Retrieved 2022-04-18, from https://www.nature.com/articles/s41586-021-04339-9 doi: 10.1038/s41586-021-04339-9

Reynolds, R. W., Smith, T. M., Liu, C., Chelton, D. B., Casey, K. S., & Schlax, M. G. (2007, November). Daily High-Resolution-Blended Analyses for Sea Surface Temperature. *Journal of Climate*, *20*(22), 5473–5496. Retrieved 2023-02-15, from http://journals.ametsoc.org/doi/10.1175/2007JCLI1824.1 doi: 10.1175/2007JCLI1824.1

Rousset, C., Vancoppenolle, M., Madec, G., Fichefet, T., Flavoni, S., Barthélemy, A., ... Vivier, F. (2015, October). The Louvain-La-Neuve sea ice model LIM3.6: global and regional capabilities. *Geoscientific Model Development*, *8*(10), 2991–3005. Retrieved 2023-02-15, from https://gmd.copernicus.org/articles/8/2991/2015/ (Publisher: Copernicus GmbH) doi: 10.5194/gmd-8-2991-2015

Rutherford, K., & Fennel, K. (2018, October). Diagnosing transit times on the northwestern North Atlantic continental shelf. *Ocean Science*, *14*(5), 1207–1221. Retrieved 2023-02-15, from https://os.copernicus.org/articles/14/1207/2018/ doi: 10.5194/os-14-1207-2018

Rutherford, K., Fennel, K., Atamanchuk, D., Wallace, D., & Thomas, H. (2021, December). A modelling study of temporal and spatial pCO_2 variability on the biologically active and temperature-dominated Scotian Shelf. *Biogeosciences*, *18*(23), 6271–6286. Retrieved 2023-02-15, from https://bg.copernicus.org/articles/18/6271/2021/ (Publisher: Copernicus GmbH) doi: 10.5194/bg-18-6271-2021

Rödenbeck, C., Keeling, R. F., Bakker, D. C. E., Metzl, N., Olsen, A., Sabine, C., & Heimann, M. (2013, March). Global surface-ocean pCO_2 and sea–air CO_2 flux variability from an observation-driven ocean mixed-layer scheme. *Ocean Science*, *9*(2), 193–216. Retrieved 2015-05-12, from http://www.ocean-sci.net/9/193/2013/ doi:

10.5194/os-9-193-2013

Schourup-Kristensen, V., Sidorenko, D., Wolf-Gladrow, D. A., & Völker, C. (2014, November). A skill assessment of the biogeochemical model REcoM2 coupled to the Finite Element Sea Ice–Ocean Model (FESOM 1.3). *Geoscientific Model Development*, *7*(6), 2769–2802. Retrieved 2023-02-15, from https://gmd.copernicus.org/articles/7/2769/2014/ doi: 10.5194/gmd-7-2769-2014

Sein, D. V., Koldunov, N. V., Danilov, S., Sidorenko, D., Wekerle, C., Cabos, W., ... Jung, T. (2018, August). The Relative Influence of Atmospheric and Oceanic Model Resolution on the Circulation of the North Atlantic Ocean in a Coupled Climate Model. *Journal of Advances in Modeling Earth Systems*, *10*(8), 2026–2041. Retrieved 2023-02-15, from http://doi.wiley.com/10.1029/2018MS001327 doi: 10.1029/2018MS001327

Seitzinger, S. P., Harrison, J. A., Dumont, E., Beusen, A. H. W., & Bouwman, A. F. (2005, December). Sources and delivery of carbon, nitrogen, and phosphorus to the coastal zone: An overview of Global Nutrient Export from Watersheds (NEWS) models and their application: GLOBAL EXPORT OF C, N, AND P TO COASTAL SYSTEMS. *Global Biogeochemical Cycles*, *19*(4), n/a–n/a. Retrieved 2023-02-15, from http://doi.wiley.com/10.1029/2005GB002606 doi: 10.1029/2005GB002606

Seland, O., Bentsen, M., Olivié, D., Toniazzo, T., Gjermundsen, A., Graff, L. S., ... Schulz, M. (2020, December). Overview of the Norwegian Earth System Model (NorESM2) and key climate response of CMIP6 DECK, historical, and scenario simulations. *Geoscientific Model Development*, *13*(12), 6165–6200. Retrieved 2023-02-15, from https://gmd.copernicus.org/articles/13/6165/2020/ doi: 10.5194/gmd-13-6165-2020

Shchepetkin, A. F., & McWilliams, J. C. (2005, January). The regional oceanic modeling system (ROMS): a split-explicit, free-surface, topography-following-coordinate oceanic model. *Ocean Modelling*, *9*(4), 347–404. Retrieved 2023-02-15, from https://www.sciencedirect.com/science/article/pii/S1463500304000484 doi: 10.1016/j.ocemod.2004.08.002

Six, K. D., & Maier-Reimer, E. (1996). Effects of plankton dynamics on seasonal carbon fluxes in an ocean general circulation model. *Global Biogeochemical Cycles*, *10*(4), 559–583. Retrieved 2023-02-15, from https://onlinelibrary.wiley.com/doi/abs/10.1029/96GB02561 doi: 10.1029/96GB02561

Stock, C. A., Dunne, J. P., Fan, S., Ginoux, P., John, J., Krasting, J. P., ... Zadeh, N. (2020). Ocean Biogeochemistry in GFDL's Earth System Model 4.1 and Its Response to Increasing Atmospheric CO2. *Journal of Advances in Modeling Earth Systems*, *12*(10), e2019MS002043. Retrieved 2021-10-11, from https://onlinelibrary.wiley.com/doi/abs/10.1029/2019MS002043 doi: 10.1029/2019MS002043

Stock, C. A., Dunne, J. P., & John, J. G. (2014, January). Global-scale carbon and energy flows through the marine planktonic food web: An analysis with a coupled physical–biological model. *Progress in Oceanography*, *120*, 1–28. Retrieved 2016-02-22, from http://www.sciencedirect.com/science/article/pii/S0079661113001079 doi: 10.1016/j.pocean.2013.07.001

Séférian, R., Nabat, P., Michou, M., Saint-Martin, D., Voldoire, A., Colin, J., ... Madec, G. (2019). Evaluation of CNRM Earth System Model, CNRM-ESM2-1: Role of Earth System Processes in Present-Day and Future Climate. *Journal of Advances in Modeling Earth Systems*, *11*(12), 4182–4227. Retrieved 2023-03-01, from https://onlinelibrary.wiley.com/doi/abs/10.1029/2019MS001791 doi: 10.1029/2019MS001791

Titchner, H. A., & Rayner, N. A. (2014, March). The Met Office Hadley Centre sea ice and sea surface temperature data set, version 2: 1. Sea ice concentrations: HADISST.2.1.0.0 SEA ICE CONCENTRATIONS. *Journal of Geophysical Research: Atmospheres*, *119*(6), 2864–2889. Retrieved 2023-02-17, from http://doi.wiley.com/10.1002/2013JD020316 doi: 10.1002/2013JD020316

Tjiputra, J. F., Schwinger, J., Bentsen, M., Morée, A. L., Gao, S., Bethke, I., ... Schulz, M. (2020, May). Ocean biogeochemistry in the Norwegian Earth System Model version 2 (NorESM2). *Geoscientific Model Development*, *13*(5), 2393–2431. Retrieved 2023-02-15, from https://gmd.copernicus.org/articles/13/2393/2020/ (Publisher: Copernicus GmbH) doi: 10.5194/gmd-13-2393-2020

Tsujino, H., Nakano, H., Sakamoto, K., Urakawa, S., Hirabara, M., Ishizaki, H., & Yamanaka, G. (2017). Reference Manual for the Meteorological Research Institute Community Ocean Model version 4(MRI.COMv4). *Technical Reports of the Meteorological Research Institute No. 80*. (10.11483/mritechrepo.80) doi: 10.11483/mritechrepo.80

Tsujino, H., Urakawa, S., Nakano, H., Small, R. J., Kim, W. M., Yeager, S. G., ... Yamazaki, D. (2018, October). JRA-55

based surface dataset for driving ocean–sea-ice models (JRA55-do). *Ocean Modelling*, *130*, 79–139. Retrieved 2023-02-15, from https://linkinghub.elsevier.com/retrieve/pii/S146350031830235X doi: 10.1016/j.ocemod.2018.07.002

Umlauf, L., & Burchard, H. (2003, March). A generic length-scale equation for geophysical turbulence models. *Journal of Marine Research*, *61*(2), 235–265. Retrieved 2023-02-15, from http://www.ingentaselect.com/rpsv/cgi-bin/cgi?ini=xref&body=linker&reqdoi=10.1357/002224003322005087 doi: 10.1357/002224003322005087

Urakawa, L. S., Tsujino, H., Nakano, H., Sakamoto, K., Yamanaka, G., & Toyoda, T. (2020, October). The sensitivity of a depth-coordinate model to diapycnal mixing induced by practical implementations of the isopycnal tracer diffusion scheme. *Ocean Modelling*, *154*, 101693. Retrieved 2023-02-15, from https://linkinghub.elsevier.com/retrieve/pii/S1463500320301955 doi: 10.1016/j.ocemod.2020.101693

Urrego-Blanco, J., & Sheng, J. (2012, September). Interannual Variability of the Circulation over the Eastern Canadian Shelf. *Atmosphere-Ocean*, *50*(3), 277–300. Retrieved 2023-02-15, from http://www.tandfonline.com/doi/abs/10.1080/07055900.2012.680430 doi: 10.1080/07055900.2012.680430

Wang, C., Zhang, L., Lee, S.-K., Wu, L., & Mechoso, C. R. (2014, March). A global perspective on CMIP5 climate model biases. *Nature Climate Change*, *4*(3), 201–205. Retrieved 2015-09-23, from http://www.nature.com/nclimate/journal/v4/n3/full/nclimate2118.html doi: 10.1038/nclimate2118

Wang, H., Hu, X., Cai, W.-J., & Sterba-Boatwright, B. (2017). Decadal fCO2 trends in global ocean margins and adjacent boundary current-influenced areas. *Geophysical Research Letters*, *44*(17), 8962–8970. Retrieved 2022-04-15, from https://onlinelibrary.wiley.com/doi/abs/10.1002/2017GL074724 doi: 10.1002/2017GL074724

Wanninkhof, R. (1992, May). Relationship between wind speed and gas exchange over the ocean. *Journal of Geophysical Research: Oceans*, *97*(C5), 7373–7382. Retrieved 2015-06-22, from http://onlinelibrary.wiley.com/doi/10.1029/92JC00188/abstract doi: 10.1029/92JC00188

Wanninkhof, R. (2014, June). Relationship between wind speed and gas exchange over the ocean revisited. *Limnology and Oceanography: Methods*, *12*(6), 351–362. Retrieved 2015-06-22, from http://onlinelibrary.wiley.com/doi/10.4319/lom.2014.12.351/abstract doi: 10.4319/lom.2014.12.351

Warner, J. C., Sherwood, C. R., Arango, H. G., & Signell, R. P. (2005, January). Performance of four turbulence closure models implemented using a generic length scale method. *Ocean Modelling*, *8*(1-2), 81–113. Retrieved 2023-02-15, from https://linkinghub.elsevier.com/retrieve/pii/S1463500303000702 doi: 10.1016/j.ocemod.2003.12.003

Weber, T., Wiseman, N. A., & Kock, A. (2019, October). Global ocean methane emissions dominated by shallow coastal waters. *Nature Communications*, *10*(1), 4584. Retrieved 2020-10-21, from https://www.nature.com/articles/s41467-019-12541-7 (Number: 1 Publisher: Nature Publishing Group) doi: 10.1038/s41467-019-12541-7

Wright, R. M., Le Quéré, C., Buitenhuis, E., Pitois, S., & Gibbons, M. J. (2021, February). Role of jellyfish in the plankton ecosystem revealed using a global ocean biogeochemical model. *Biogeosciences*, *18*(4), 1291–1320. Retrieved 2023-03-27, from https://bg.copernicus.org/articles/18/1291/2021/ (Publisher: Copernicus GmbH) doi: 10.5194/bg-18-1291-2021

Wu, H., & Zhu, J. (2010, January). Advection scheme with 3rd high-order spatial interpolation at the middle temporal level and its application to salt-water intrusion in the Changjiang Estuary. *Ocean Modelling*, *33*(1-2), 33–51. Retrieved 2023-02-15, from https://linkinghub.elsevier.com/retrieve/pii/S1463500309002121 doi: 10.1016/j.ocemod.2009.12.001

Yang, S., Chang, B. X., Warner, M. J., Weber, T. S., Bourbonnais, A. M., Santoro, A. E., ... Bianchi, D. (2020, June). Global reconstruction reduces the uncertainty of oceanic nitrous oxide emissions and reveals a vigorous seasonal cycle. *Proceedings of the National Academy of Sciences*, *117*(22), 11954–11960. Retrieved 2022-05-12, from https://www.pnas.org/doi/10.1073/pnas.1921914117 (Publisher: Proceedings of the National Academy of Sciences) doi: 10.1073/pnas.1921914117

Yukimoto, S., Kawai, H., Koshiro, T., Oshima, N., Yoshida, K., Urakawa, S., ... Ishii, M. (2019). The Meteorological Research Institute Earth System Model Version 2.0, MRI-ESM2.0: Description and Basic Evaluation of the Physical Component. *Journal of the Meteorological Society of Japan. Ser. II*, *97*(5), 931–965. Retrieved 2023-02-15, from https://www.jstage.jst.go.jp/article/jmsj/97/5/97_2019-051/_article doi: 10.2151/jmsj.2019-051

Zweng, M. M., Reagan, J. R., Antonov, J. I., Lo-

carnini, R. A., Mishonov, A. V., Boyer, T. P., ... Biddle, M. (2014). *World Ocean Atlas 2013, Volume 2: Salinity.* (Tech. Rep.). S. Levitus, Ed., A. Mishonov Technical Ed.; NOAA Atlas NESDIS 74, 39 pp.